Supporting Information

Simple Colorimetric and Fluorescence Chemosensing Probe for Selective Detection of Sn^{2+} Ions in an Aqueous Solution: Evaluation of the Novel Sensing Mechanism and Its Bioimaging Applications

Palanisamy Ravichandiran,[†] Vignesh Krishnamoorthi Kaliannagounder,[‡,Δ] Antony Paulraj Bella,[§] Anna Boguszewska-Czubara,[#] Maciej Masłyk,[¶] Cheol Sang Kim,[‡,ǂ] Chan Hee Park,[‡,ǂ] Princy Merlin Johnson,[§] Byung-Hyun Park,[ǁ] Myung-Kwan Han,[※] Ae Rhan Kim,[†,±] and Dong Jin Yoo[*,†,±]

[†] Department of Life Sciences, College of Natural Sciences, Jeonbuk National University, 567 Baekje-daero, Deokjin-gu, Jeonju-si, Jeollabuk-do 54896, Republic of Korea.
[‡] Department of Bionanotechnology and Bioconvergence Engineering, Graduate School, Jeonbuk National University, 567 Baekje-daero, Deokjin-gu, Jeonju-si, Jeollabuk-do 54896, Republic of Korea.
[Δ] Department of Bionanosystem Engineering, Graduate School, Jeonbuk National University, 567 Baekje-daero, Deokjin-gu, Jeonju-si, Jeollabuk-do 54896, Republic of Korea.
[§] PG and Research Department of Chemistry, Bishop Heber College, Vayalur Road, Puthur, Tiruchirappalli-620017, Tamil Nadu, India.
[#] Department of Medical Chemistry, Medical University of Lublin, ul. Chodźki 4A, 20-093, Lublin, Poland.
[¶] Department of Molecular Biology, Faculty of Biotechnology and Environmental Sciences, The John Paul II Catholic University of Lublin, ul. Konstantynów 1i, 20-708 Lublin, Poland.
[ǂ] Mechanical Design Engineering, Jeonbuk National University, 567 Baekje-daero, Deokjin-gu, Jeonju-si, Jeollabuk-do 54896, Republic of Korea.
[ǁ] Department of Biochemistry, Jeonbuk National University Medical School, 567 Baekje-daero, Deokjin-gu, Jeonju-si, Jeollabuk-do 54896, Republic of Korea.
[※] Department of Microbiology, Jeonbuk National University Medical School, 567 Baekje-daero, Deokjin-gu, Jeonju-si, Jeollabuk-do 54896, Republic of Korea.
[±] Department of Energy Storage/Conversion Engineering of Graduate School, and Hydrogen and Fuel Cell Research Center, Jeonbuk National University, 567 Baekje-daero, Deokjin-gu, Jeonju-si, Jeollabuk-do 54896, Republic of Korea.
[*]**Corresponding Author Email**: djyoo@jbnu.ac.kr (Dong Jin Yoo)

Table of Contents

Synthesis and Spectroscopic Data of Sensor Probe 4CBS

General

Melting point (ºC) of the sensor probe **4CBS** was analyzed by with a digital melting point apparatus (Stuart, SMP10, Staffordshire, ST15 OSA, UK). All the chemicals were purchased from Alfa Aesar/Sigma-Aldrich, Korea. The UV/vis spectrum was performed in a diode-array spectrophotometer (Hewlett Packard 8453 (G1103A), quartz cuvette, cell length 1 cm). The emission spectrum was performed in fluorescence spectrometer with a slit width of 5/5 (JASCO, FP-6500). The synthesized sensor probe was carefully characterized by FT-IR (Perkin-Elmer, Frontier MIR/FIR Spectrometer, L1280044, ATR/KBr method), ^{1}H NMR (500 MHz, Jeol), ^{13}C NMR (150 MHz, Jeol) and mass (ESI) spectral investigations (LC-MS, Agilent 1100). Elemental analysis was carried in CHNS/O Analyzers (FLASH 2000, Thermo Fisher Scientific). The cyclic voltammetry study was performed in an electrochemical workstation (GAMRY Reference 600). Topographies of the metal complex were analyzed by atomic force microscopy (AFM) (multimode-8 model). Images were recorded in contact mode with 300 kHz cantilever frequency that equipped with antimony doped silicon tip (radius = 20 nm, spring constant = 40 N m^{-1}). Dynamic light scattering (DLS) experiments were carried out in a Brookhaven 90 Plus nanoparticle size analyzer instrument. Quantum chemical calculations (DFT) were carried out at the B3LYP/6-31G (d,p) and B3LYP/ LANL2DZ /6-31G(d,p) level using the Gaussian 16 program.[1] For bioimaging studies, DIC images were captured under the white LED source. Fluorescence bioimaging studies were performed under green filter (excitation = 488 nm; emission = 548 nm) and red filter (excitation = 594 nm; emission = 654 nm).

Preparation of Ligand 4CBS

2,3-Dichloro-1,4-naphthoquinone **1** (3.405 g, 15 mM) and *p*-aminobenzenesulfonamide **2** (2.58 g, 15 mM) were dispersed in double-distilled water (900 mL). The reaction mixture was refluxed for 3 h with constant stirring. The completion of the reaction was confirmed by thin-layer chromatography (ethyl acetate: hexane 1:1, v/v). The reaction mixture was partially cooled at room temperature and the obtained precipitate was isolated by *vacuum* filtration. The obtained crude product was thoroughly washed with hot water (900 mL) and dried at 45 ºC. The isolated crude sample was additionally purified by column chromatography (silica gel, 100–200 mesh, ethyl acetate: hexane 1:1) to give the desired ligand **4CBS**. Orange solid (98%); mp: >300 ºC; IR (KBr) $\tilde{\nu}$ = 694, 742, 1015, 1095, 1163, 1288, 1514, 1571, 1636, 1677, 3220, 3350 cm^{-1}. ^{1}H NMR (500 MHz, DMSO-d_6, 25 °C, TMS): δ = 7.22 (d, J = 10.7 Hz, 2H), 7.30 (s, 2H), 7.72 (d, J = 10.7 Hz, 2H), 7.82 (dt, J = 9.3 Hz & J = 0.9 Hz, 1H), 7.88 (dt, J = 9.1 Hz & J = 1.9 Hz, 1H), 8.04 (d, J = 10.3 Hz, 2H), 9.54 (s, 1H) ppm. ^{13}C NMR (150 MHz, DMSO-d_6): δ = 117.8, 122.3, 125.7, 126.2, 126.5, 130.4, 131.7, 133.4, 134.7, 138.5, 142.2, 142.7, 176.9, 179.9 ppm. MS (ESI) m/z: calcd for $C_{16}H_{11}ClN_2O_4S$, $[M + H]^+$ 362.78, found: 363.55. Anal. calcd for $C_{16}H_{11}ClN_2O_4S$ (362): C, 52.97; H, 3.06; N, 7.72; S, 8.84. Found: C, 52.65; H, 3.13; N, 7.59; S, 9.02; Beilstein test: Cl positive.[2]

^{1}H NMR and ^{13}C NMR Spectra of Ligand 4CBS

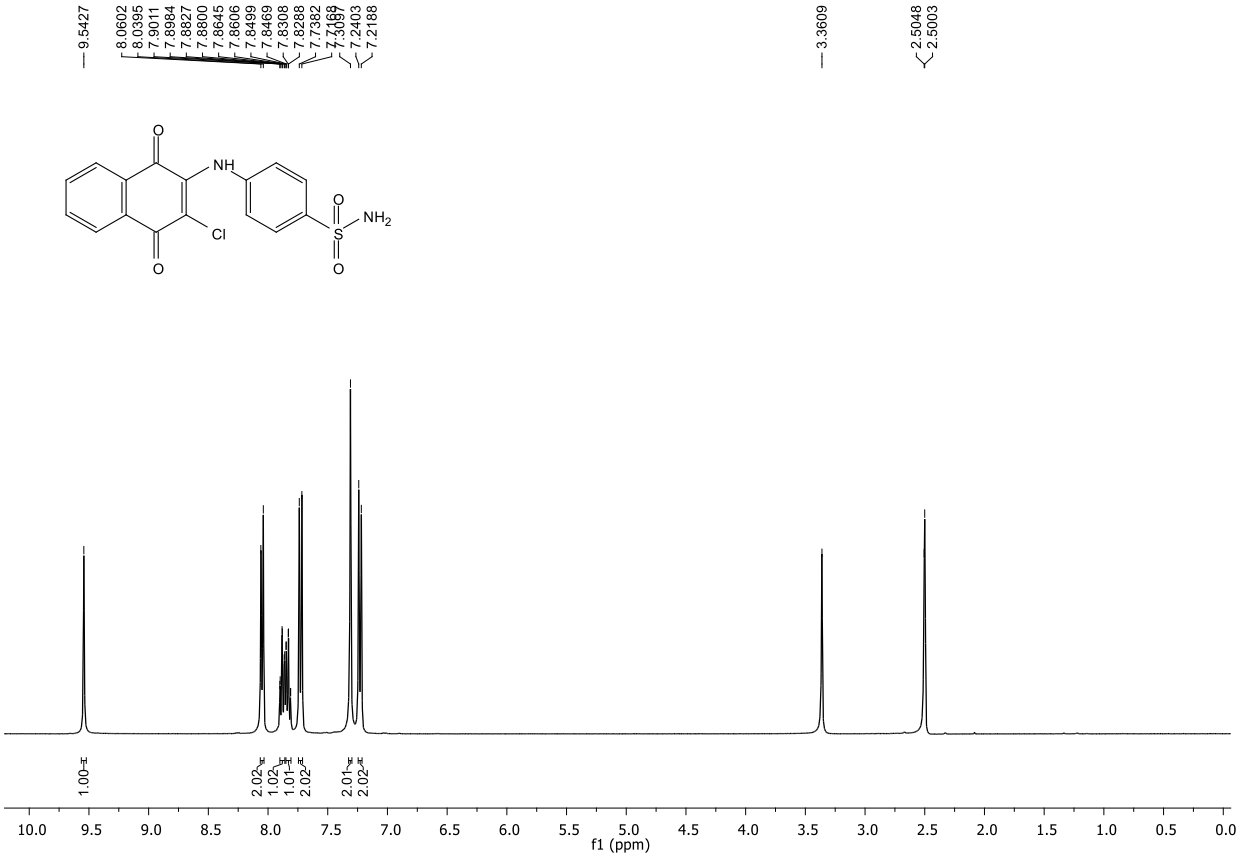

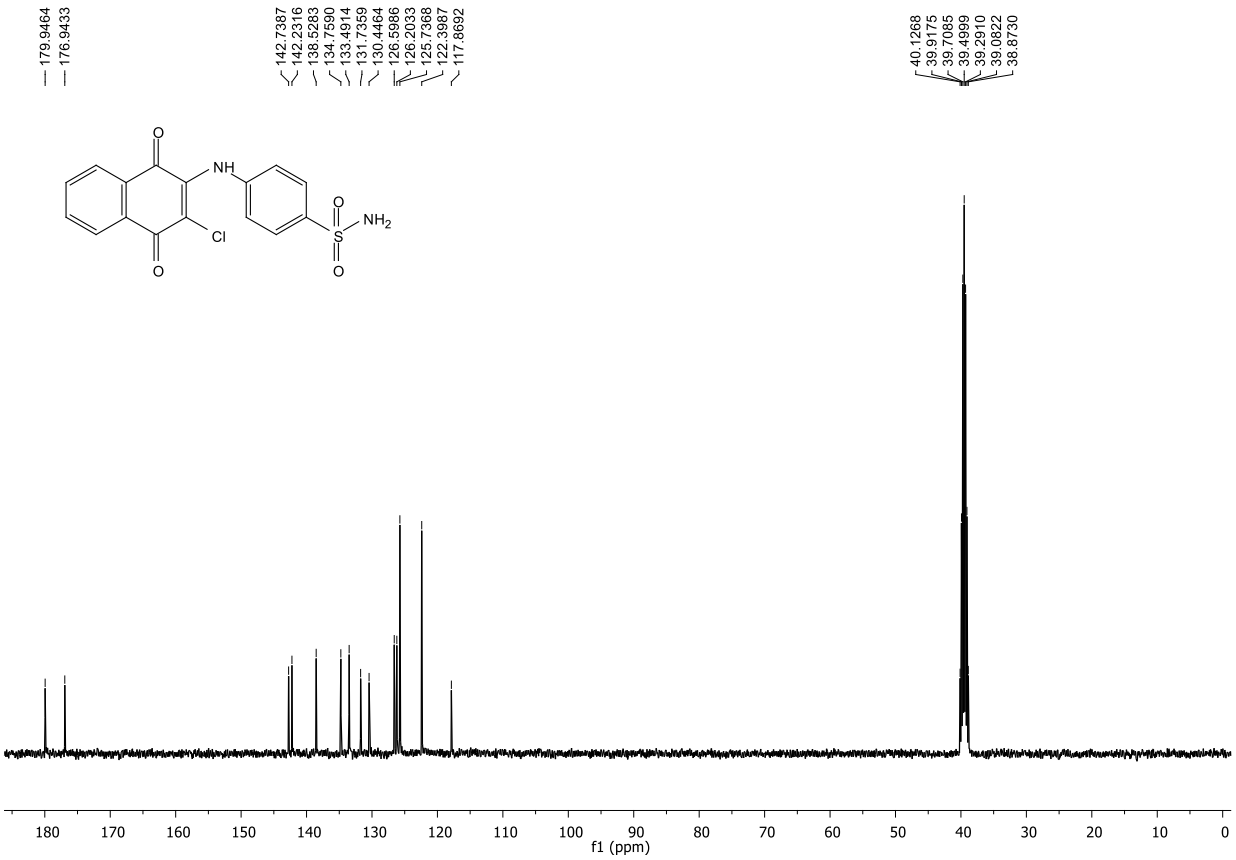

Figure S1. ^{1}H NMR and ^{13}C NMR spectra of ligand **4CBS**

Mass (ESI) Spectra of Ligand 4CBS

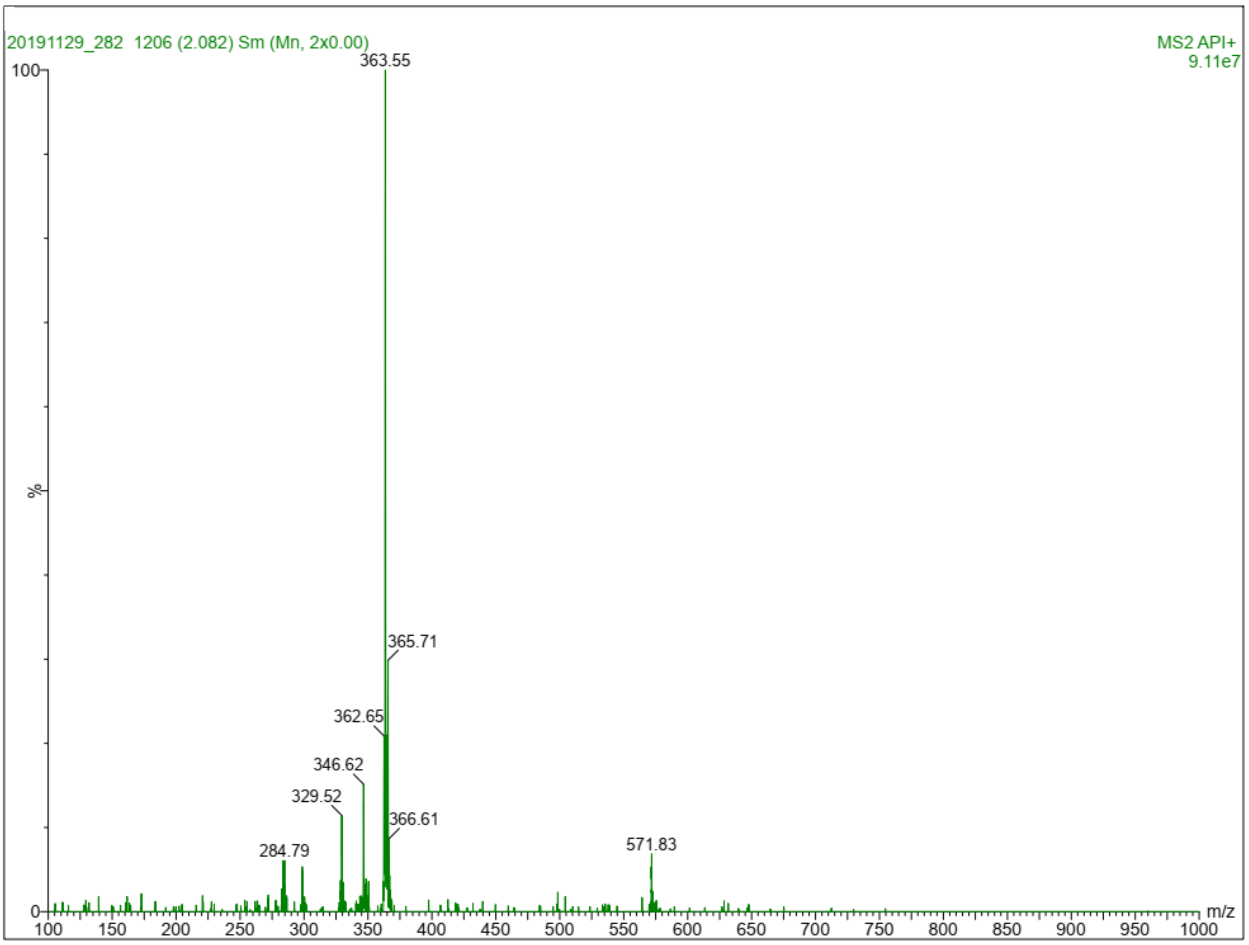

Figure S2. ESI-Mass spectrum of ligand **4CBS** in methanol.

Solvatochromic Study of the Chemosensing Probe 4CBS

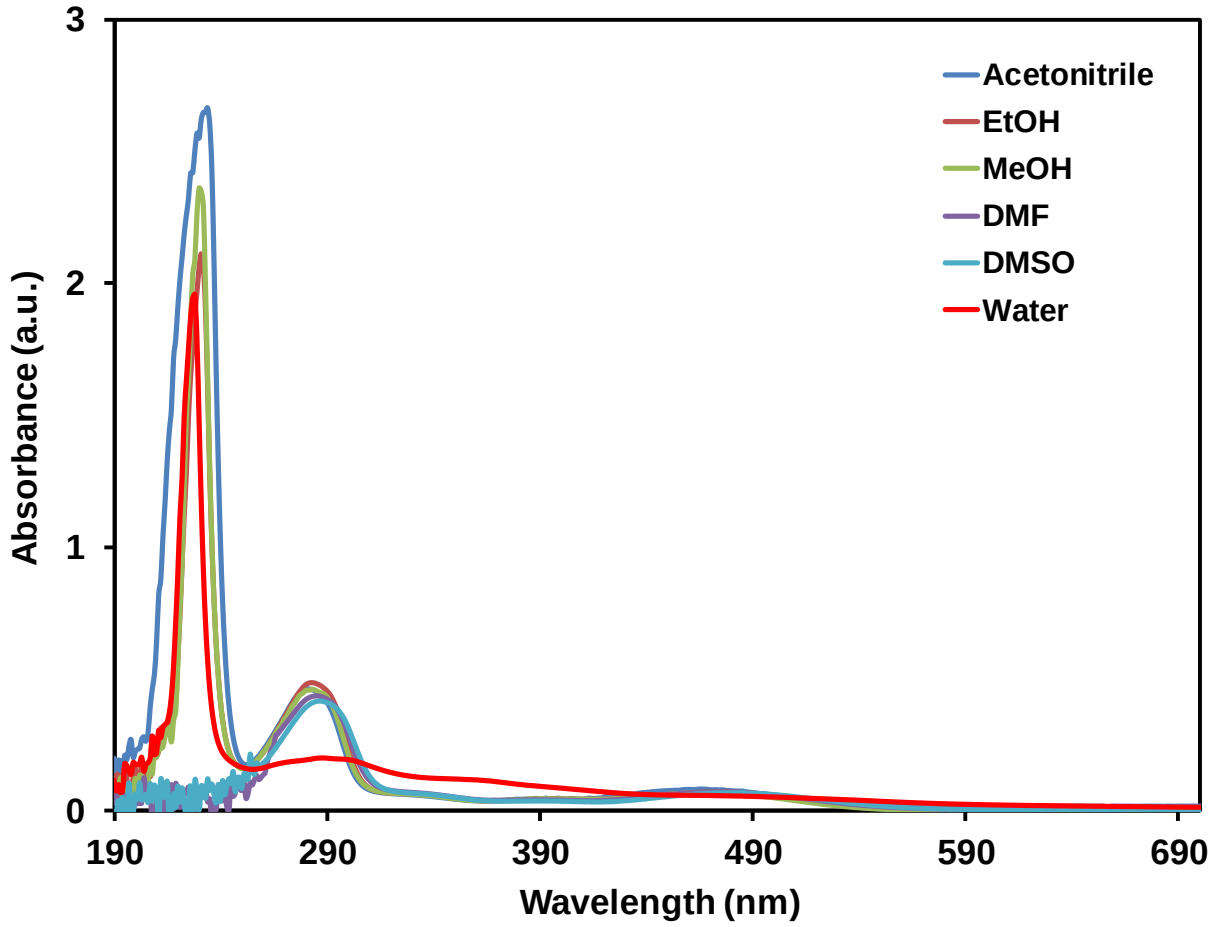

Figure S3. UV/vis study of **4CBS** (1.25×10^{-5} M) in different organic solvents and water (20 mM HEPES, pH = 7.5).

Fluorescence Emission Spectra of 4CBS–Sn^{2+} Complex at Different Excitation Wavelengths

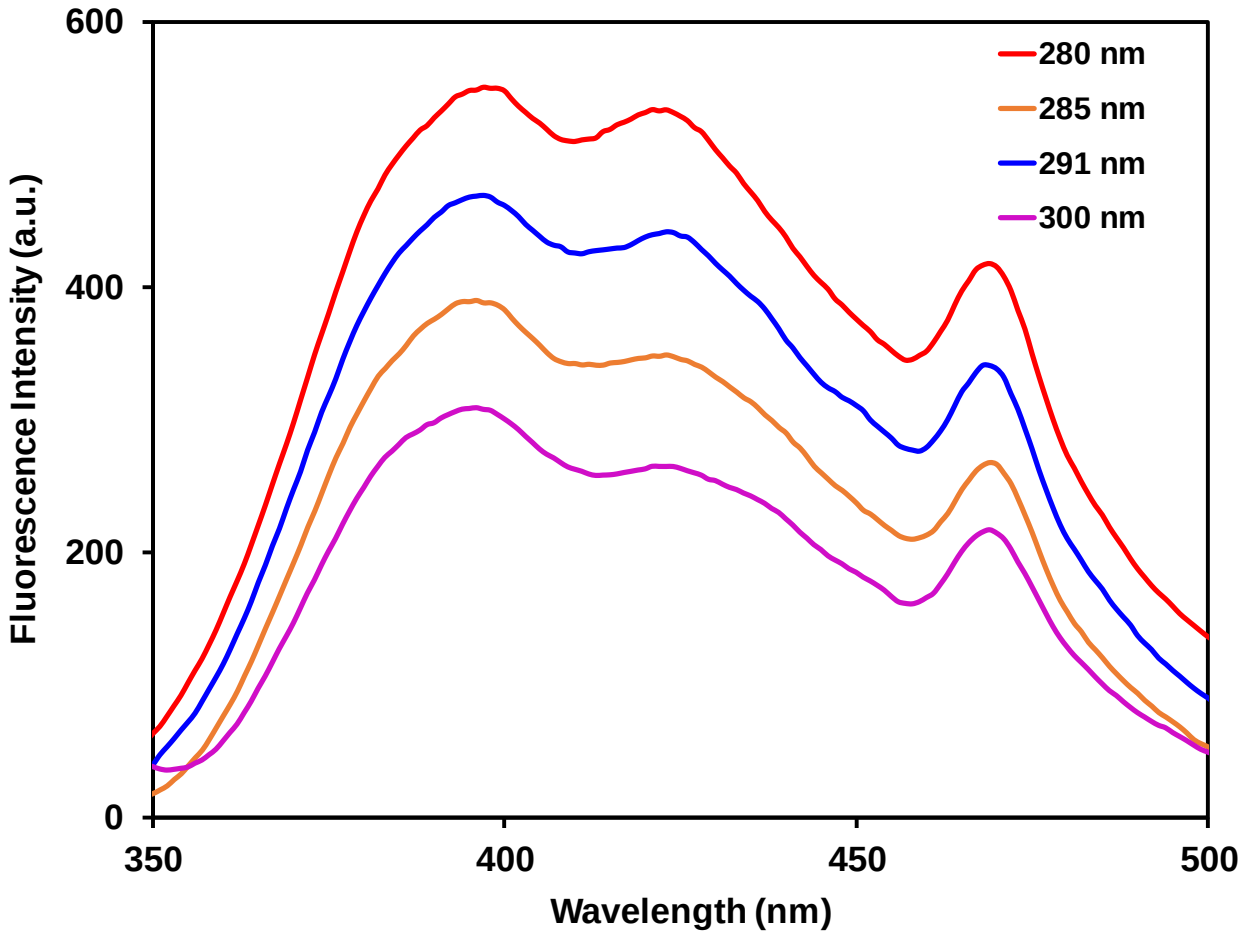

Figure S4. Fluorescence emission study of **4CBS** (1.25×10^{-5} M) in the presence of Sn^{2+} (2.50×10^{-4} M) at various excitation wavelengths in the aqueous solution (20 mM HEPES, pH = 7.5).

DLS Analysis of 4CBS–Sn^{2+} Complex

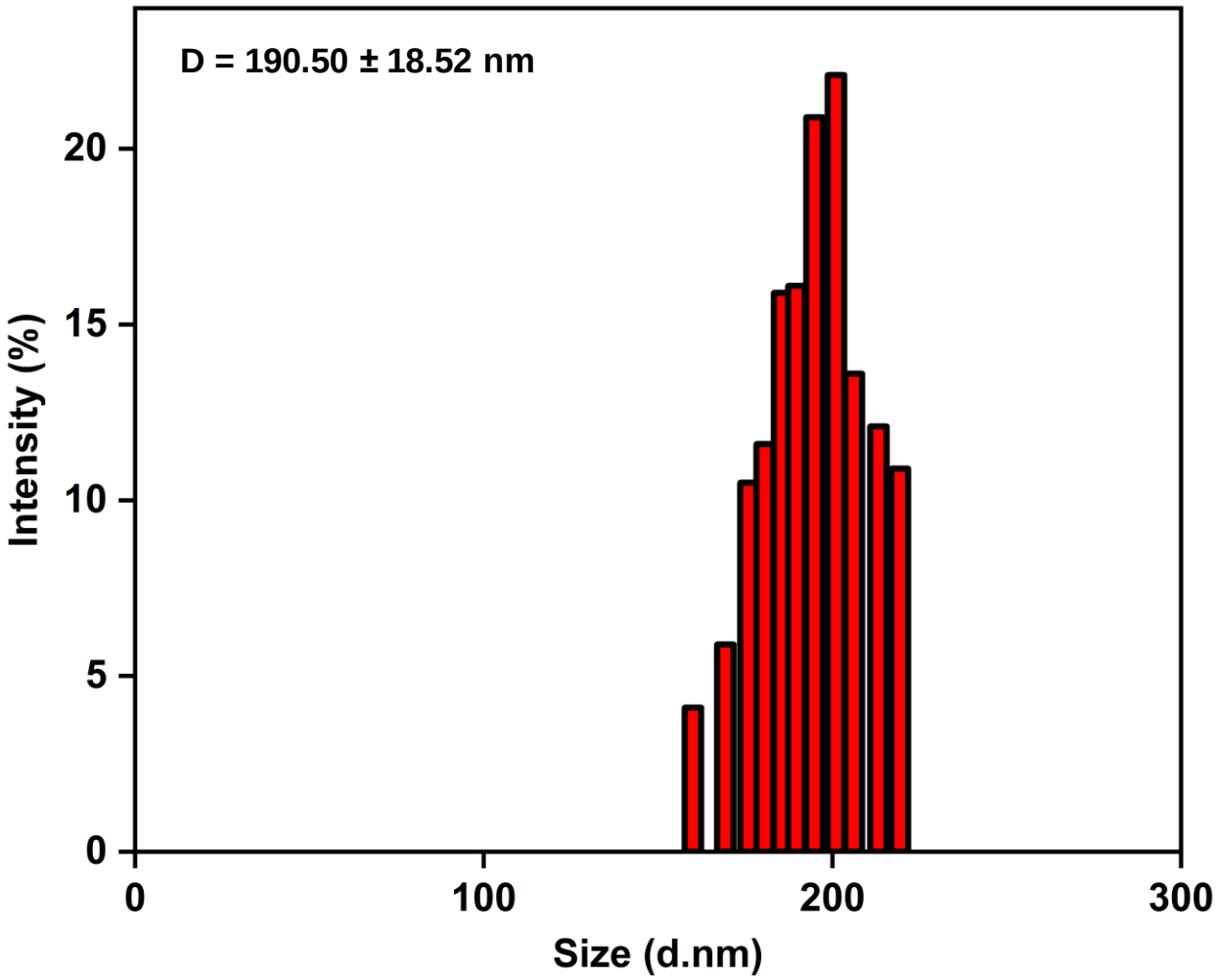

Figure S5. DLS analysis of **4CBS** (1.25×10^{-5} M) with Sn^{2+} (5.0×10^{-4} M) in the aqueous solution (20 mM HEPES, pH = 7.5).

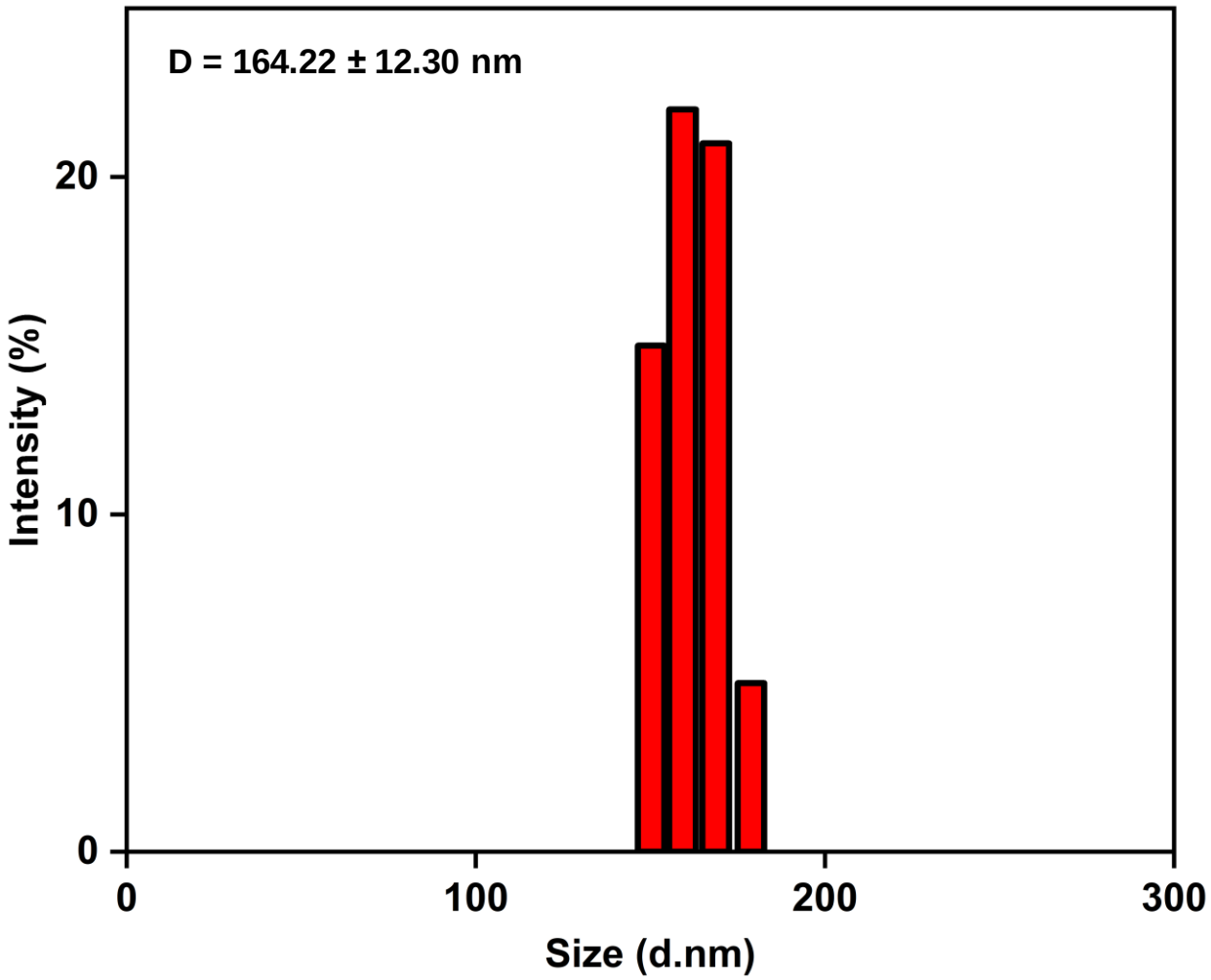

Figure S6. DLS analysis of **4CBS** (1.25×10^{-5} M) with Sn^{2+} (1.25×10^{-3} M) in the aqueous solution (20 mM HEPES, pH = 7.5).

AFM Morphological Analysis of 4CBS–Sn^{2+} Complex

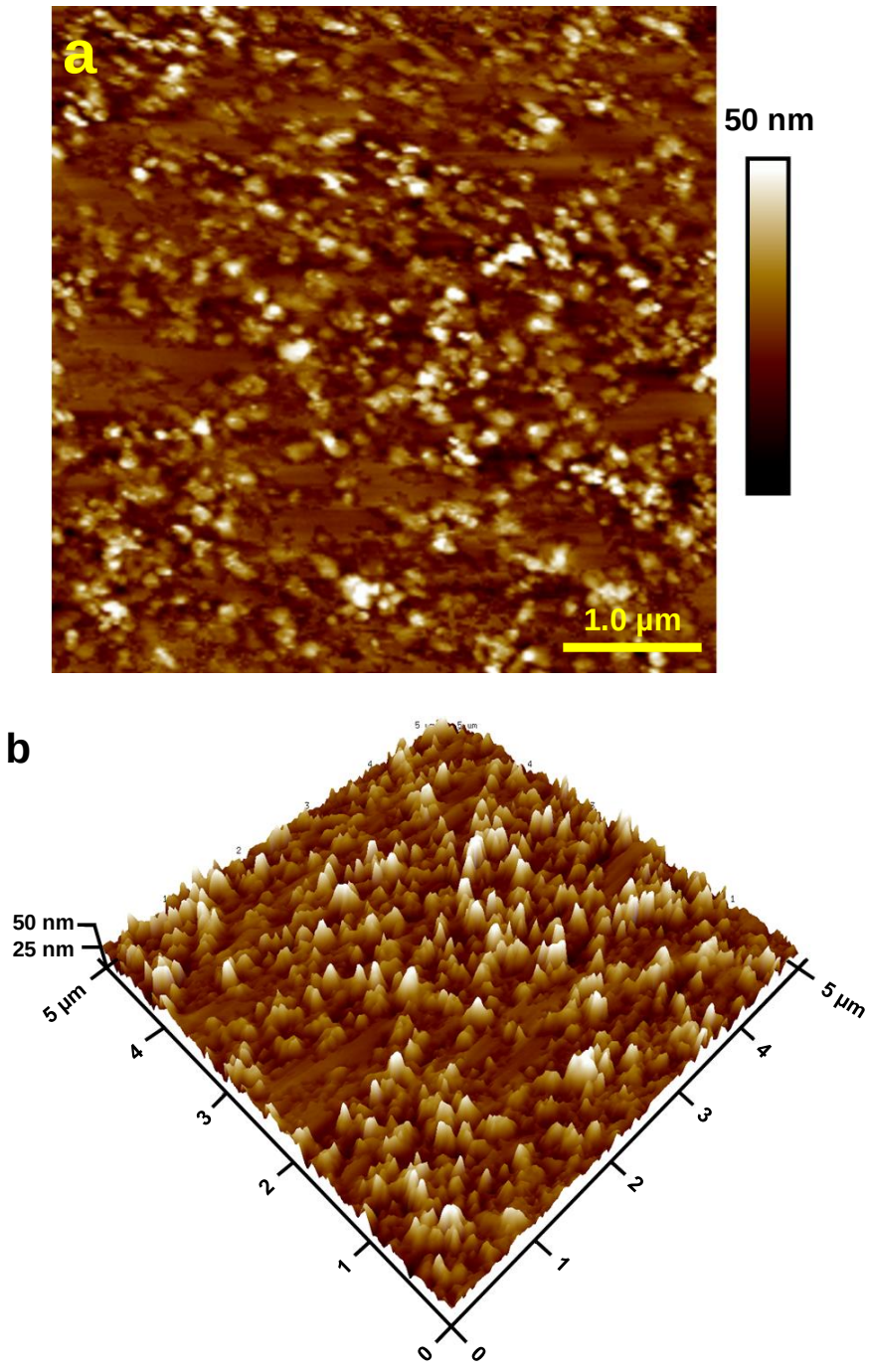

Figure S7. AFM topography of **4CBS** (1.25×10^{-5} M) with Sn^{2+} (5.0×10^{-4} M) in the aqueous solution (20 mM HEPES, pH = 7.5); where (a) 2D image of **4CBS** with Sn^{2+}; (b) 3D image of **4CBS** with Sn^{2+}.

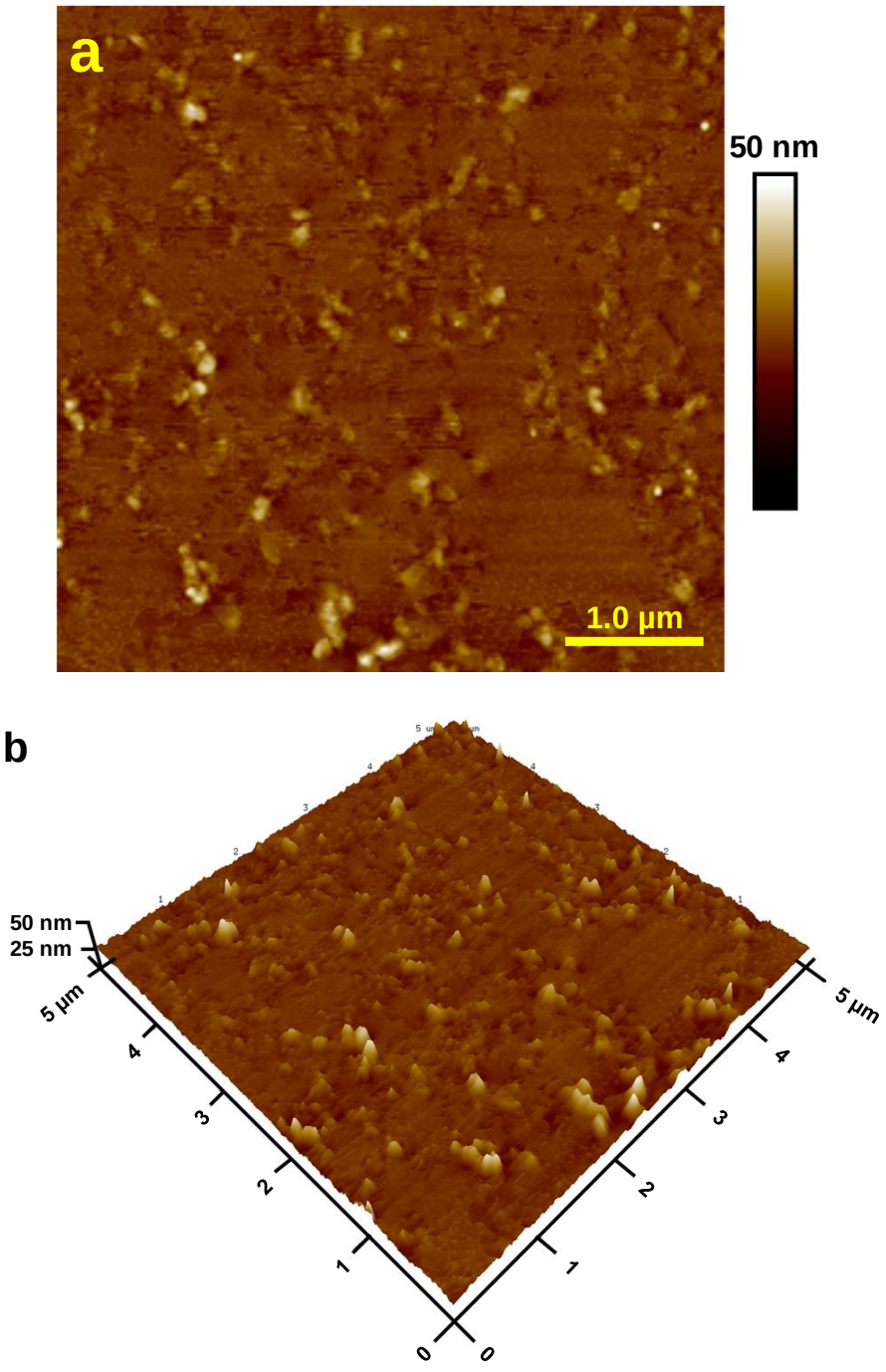

Figure S8. AFM topography of **4CBS** (1.25×10^{-5} M) with Sn^{2+} (1.25×10^{-3} M) in the aqueous solution (20 mM HEPES, pH = 7.5); where (a) 2D image of **4CBS** with Sn^{2+}; (b) 3D image of **4CBS** with Sn^{2+}.

Effect of Aggregates/Precipitates Induced Fluorescence Emission in 4CBS–Sn^{2+} Complex

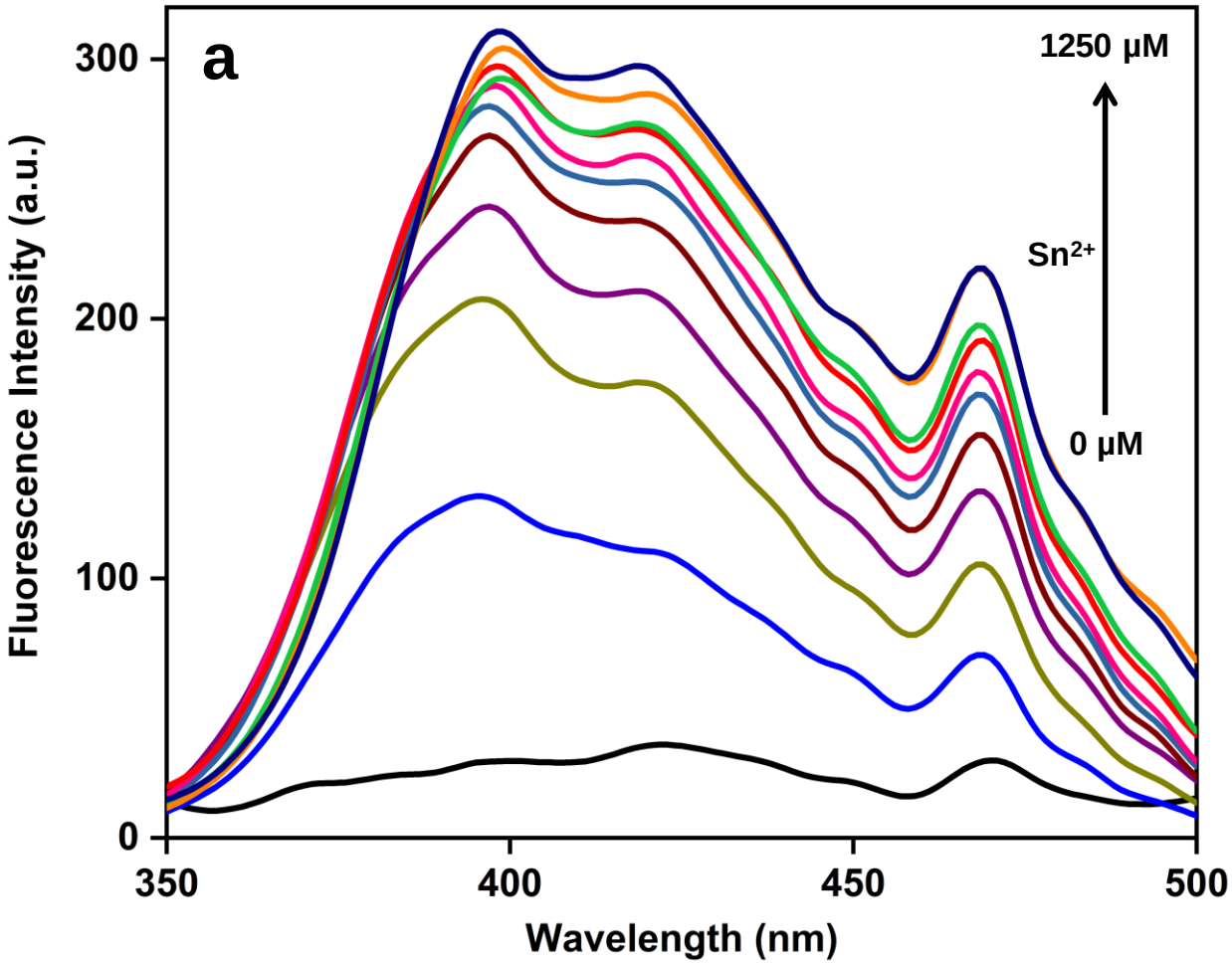

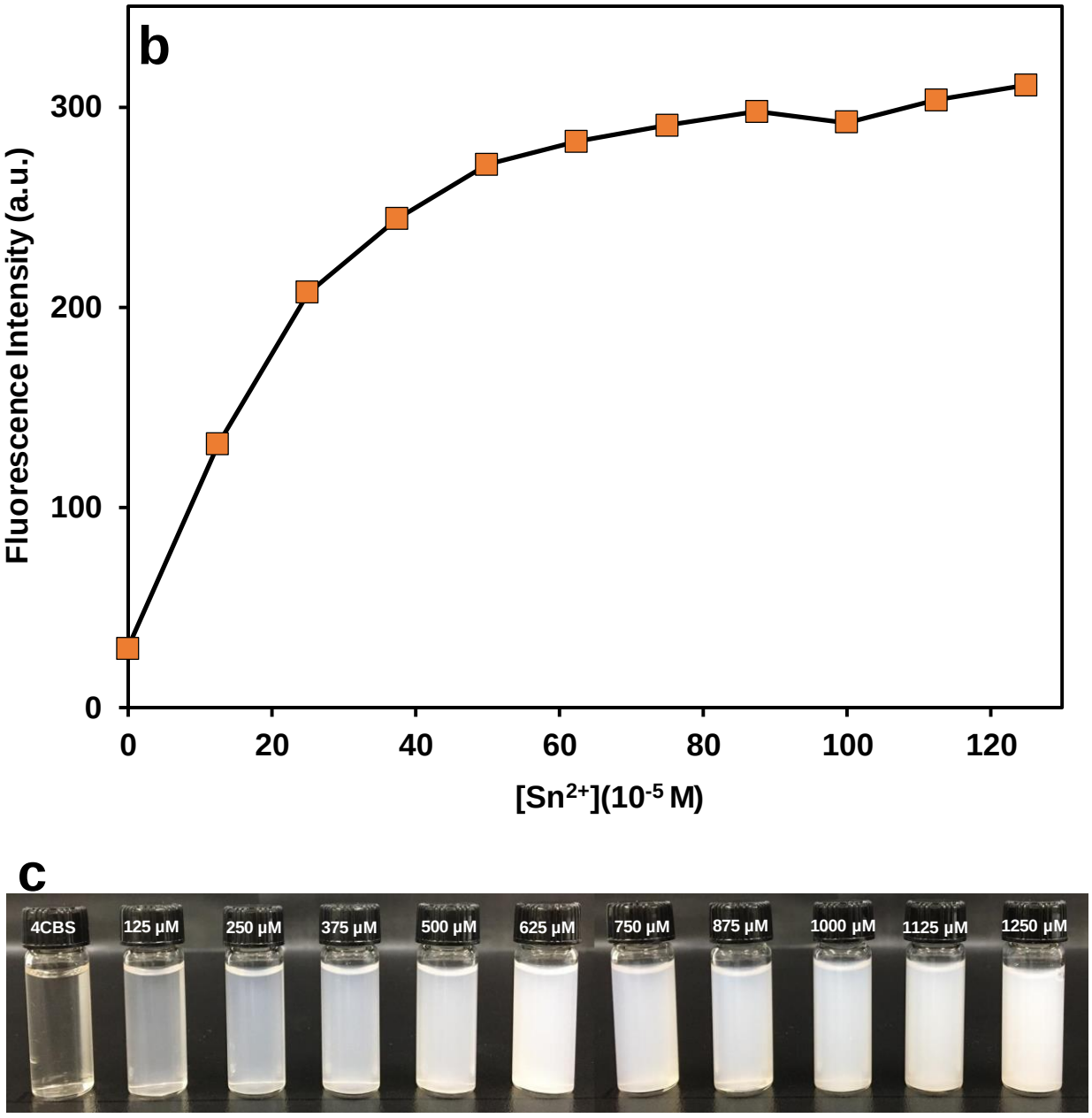

Figure S9. Study of aggregates/precipitates induced fluorescence emission in **4CBS**–Sn^{2+} complex; where (a) fluorescence emission spectra of **4CBS** with the increased concentration of Sn^{2+} (0 M to 1.25×10^{-3} M) in the aqueous solution (20 mM HEPES, pH = 7.5), slit width 3/5; (b) plot of fluorescence emission intensity of **4CBS** vs. increased concentration of Sn^{2+}; (c) image of colorimetric changes of **4CBS** with the increased concentration of Sn^{2+}.

Effect of Water in CH_3CN Solution of 4CBS

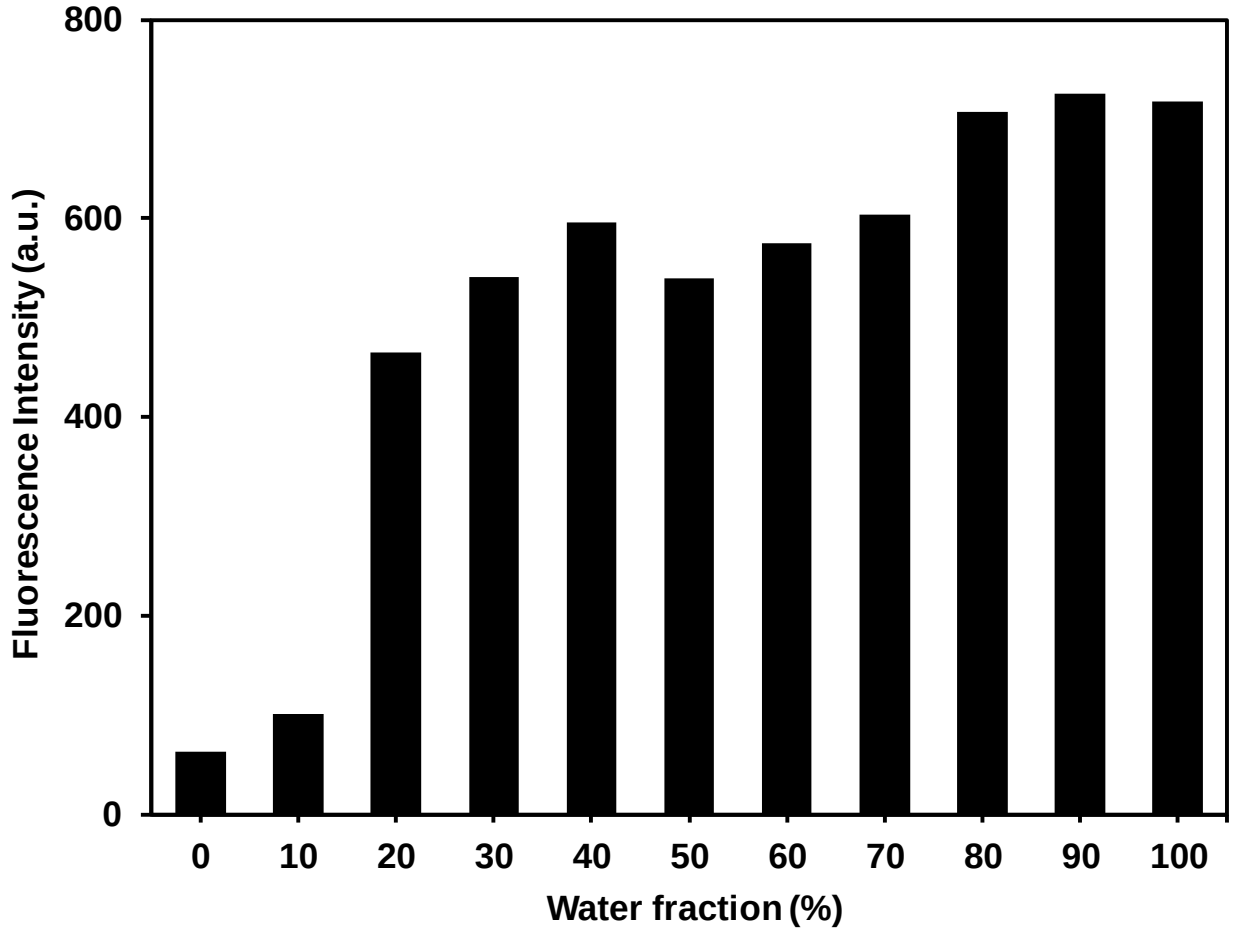

Figure S10. Fluorescence intensity of **4CBS** (1.25×10^{-5} M) – Sn^{2+} (2.50×10^{-4} M) complex in CH_3CN with the increased amount of water (20 mM HEPES, pH = 7.5), λ_{ex} = 280 nm; λ_{em} = 397 nm.

Effect of HEPES Buffer in the Aqueous 4CBS

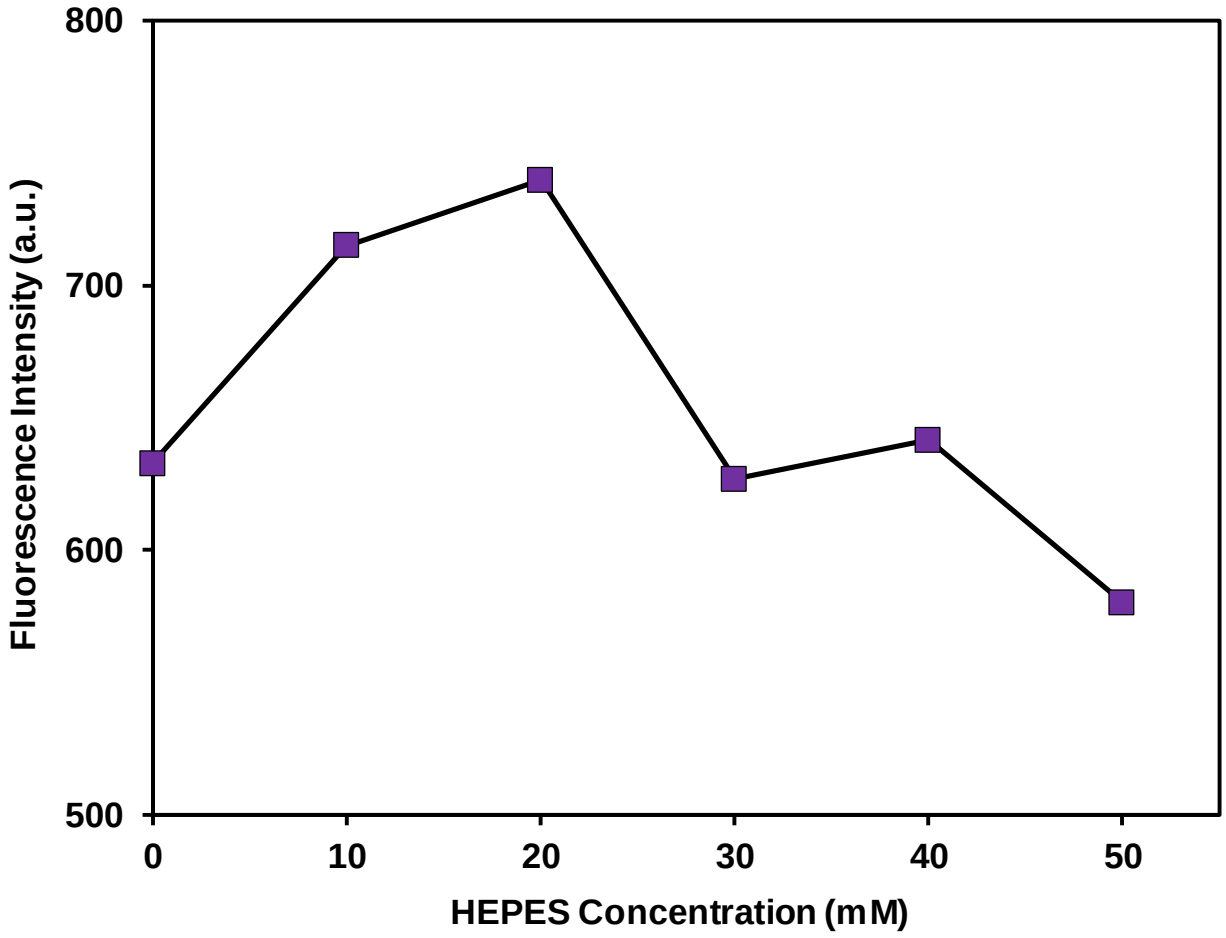

Figure S11. Fluorescence intensity of **4CBS** (1.25×10^{-5} M) – Sn^{2+} (2.50×10^{-4} M) complex in water with the incremental addition of HEPES buffer (pH = 7.5), λ_{ex} = 280 nm; λ_{em} = 397 nm.

Effects of Solvents in 4CBS–Sn^{2+}Complex

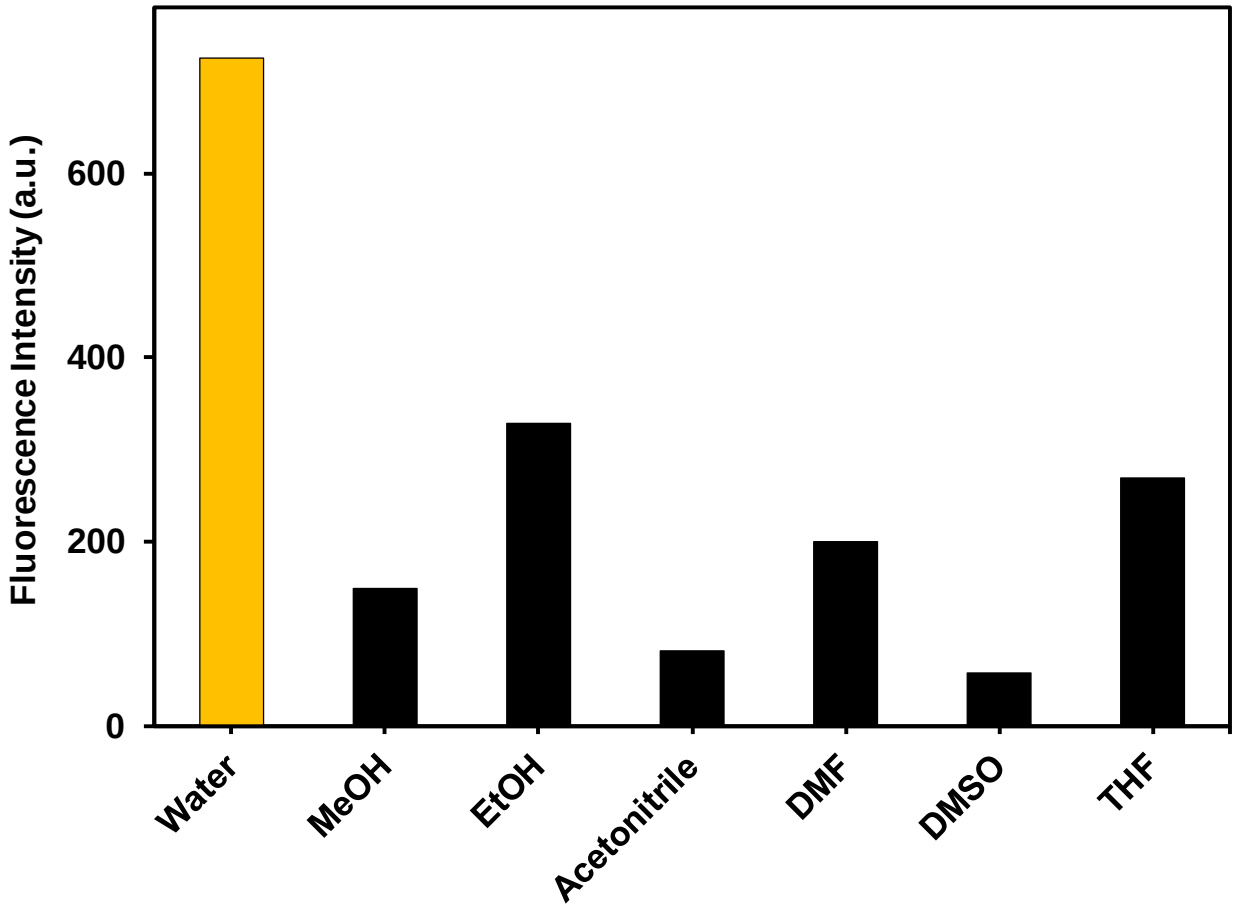

Figure S12. The solvent effects of **4CBS** (1.25×10^{-5} M) with Sn^{2+} (2.50×10^{-4} M) in various organic solvents and water (20 mM HEPES, pH = 7.5), λ_{ex} = 280 nm; λ_{em} = 397 nm.

Linear Relationship Curve of 4CBS

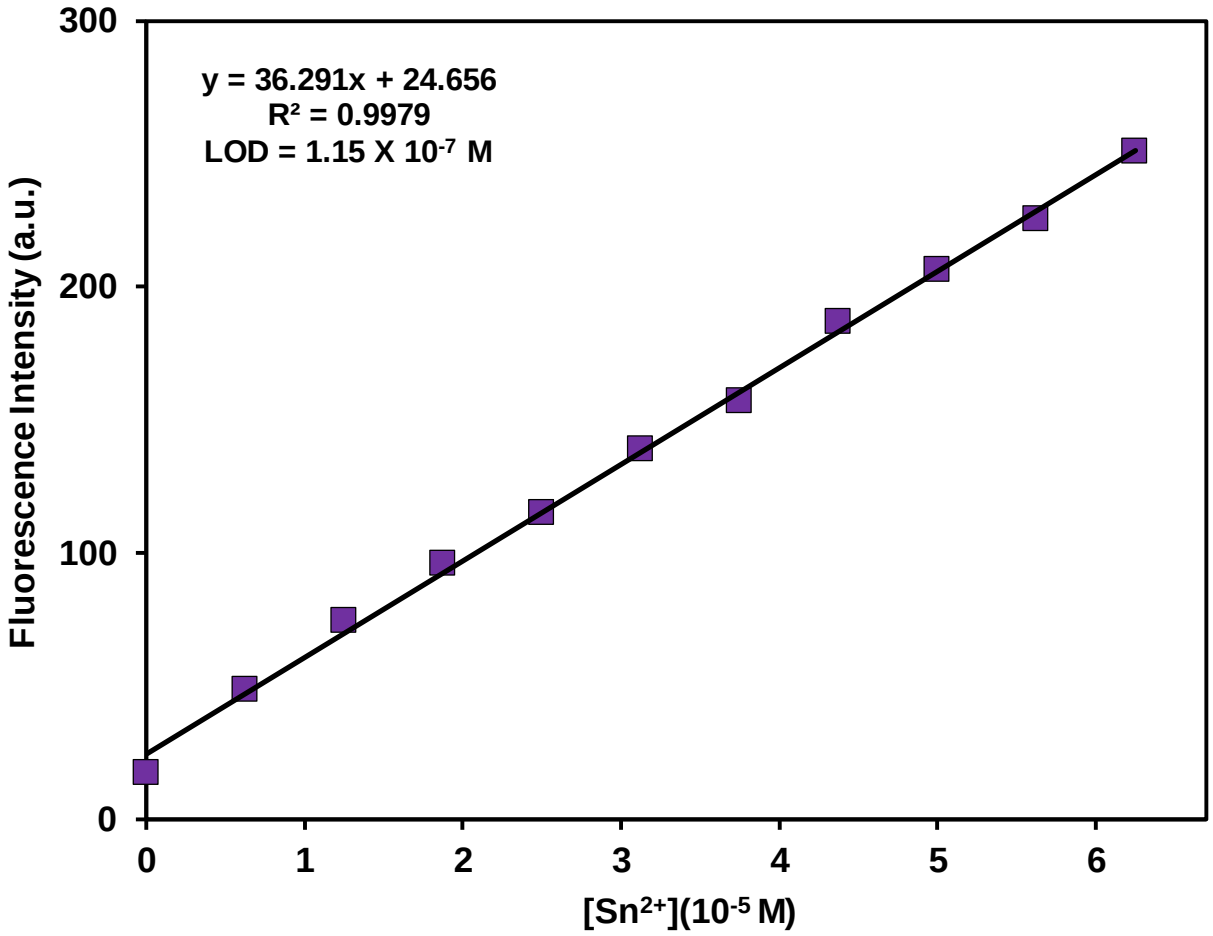

Figure S13. Linear relationship curve of **4CBS** (1.25×10^{-5} M) with the increasing concentration of Sn^{2+} (0 M to 6.25×10^{-5} M) in the aqueous solution (20 mM HEPES, pH = 7.5), λ_{ex} = 280 nm; λ_{em} = 397 nm.

Fluorescence Metal Ion Selectivity Analysis of 4CBS–Sn^{2+}Complex

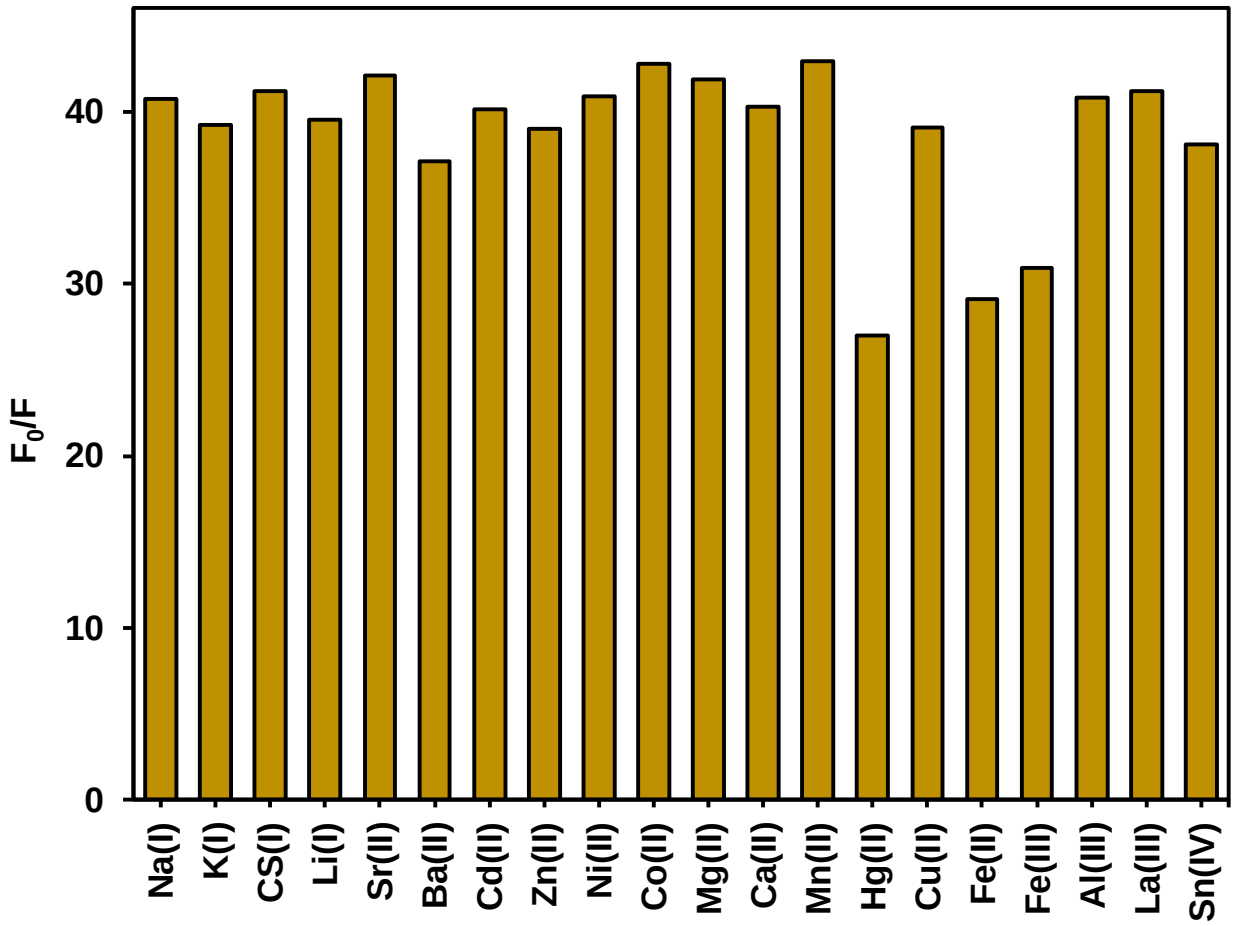

Figure S14. Selectivity study of **4CBS** for Sn^{2+} with different interfering metal cations. The graph plotted from the ratio of the slope of the calibration plot for Sn^{2+} (0 M to 6.25×10^{-5} M) to the slope of a plot for a given metal cation interference (0 M to 6.25×10^{-5} M); where F_0 = slope of the calibration plot of Sn^{2+}; F = slope of the calibration plot of the other metal ions in the aqueous solution (20 mM HEPES, pH = 7.5), λ_{ex} = 280 nm; λ_{em} = 397 nm.

UV/vis Metal Ion Interference Study of 4CBS–Sn^{2+}Complex

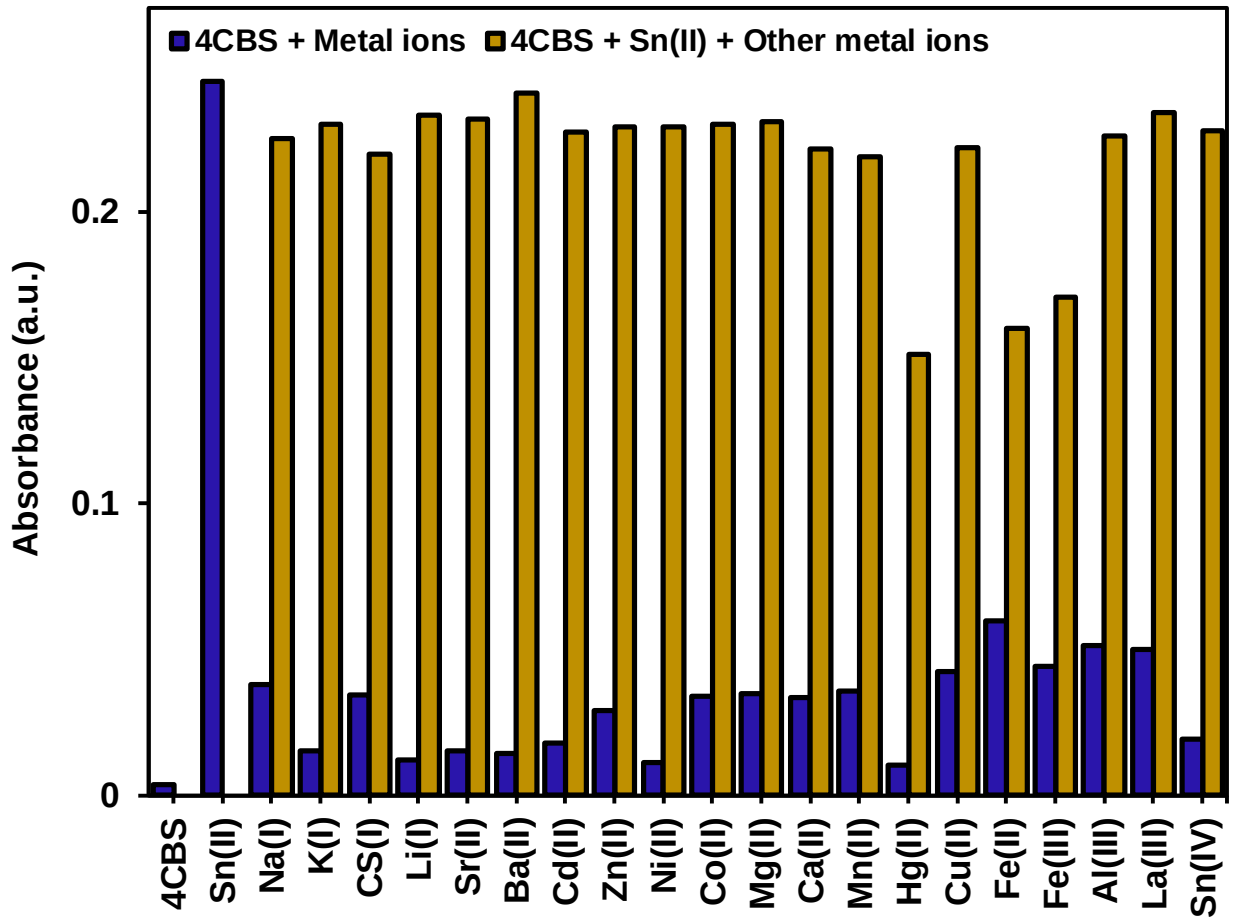

Figure S15. UV/vis metal ion interference study of **4CBS** (1.25×10^{-5} M) and Sn^{2+} (1.25×10^{-4} M) with the co-existence of other metal ions (1.25×10^{-4} M) in the aqueous solution (20 mM HEPES, pH = 7.5); λ_{max} = 488 nm.

Job's Plot Analysis of 4CBS–Sn^{2+}Complex

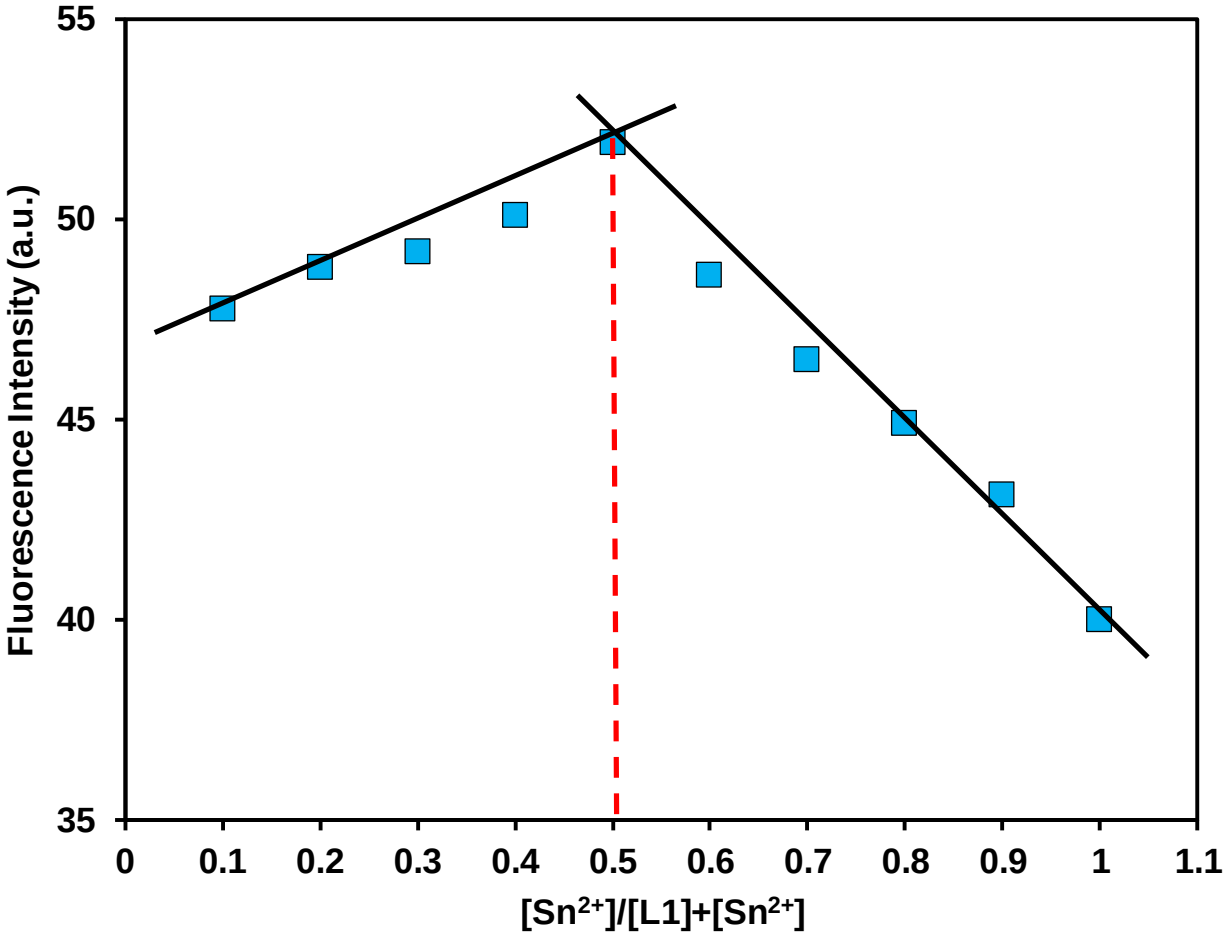

Figure S16. Job's plot analysis of **4CBS**–Sn^{2+} complex for 1:1 binding stoichiometry in the aqueous solution (20 mM HEPES, pH = 7.5), λ_{ex} = 280 nm; λ_{em} = 397 nm.

Mass (ESI) spectrum of 4CBS–Sn^{2+} Complex

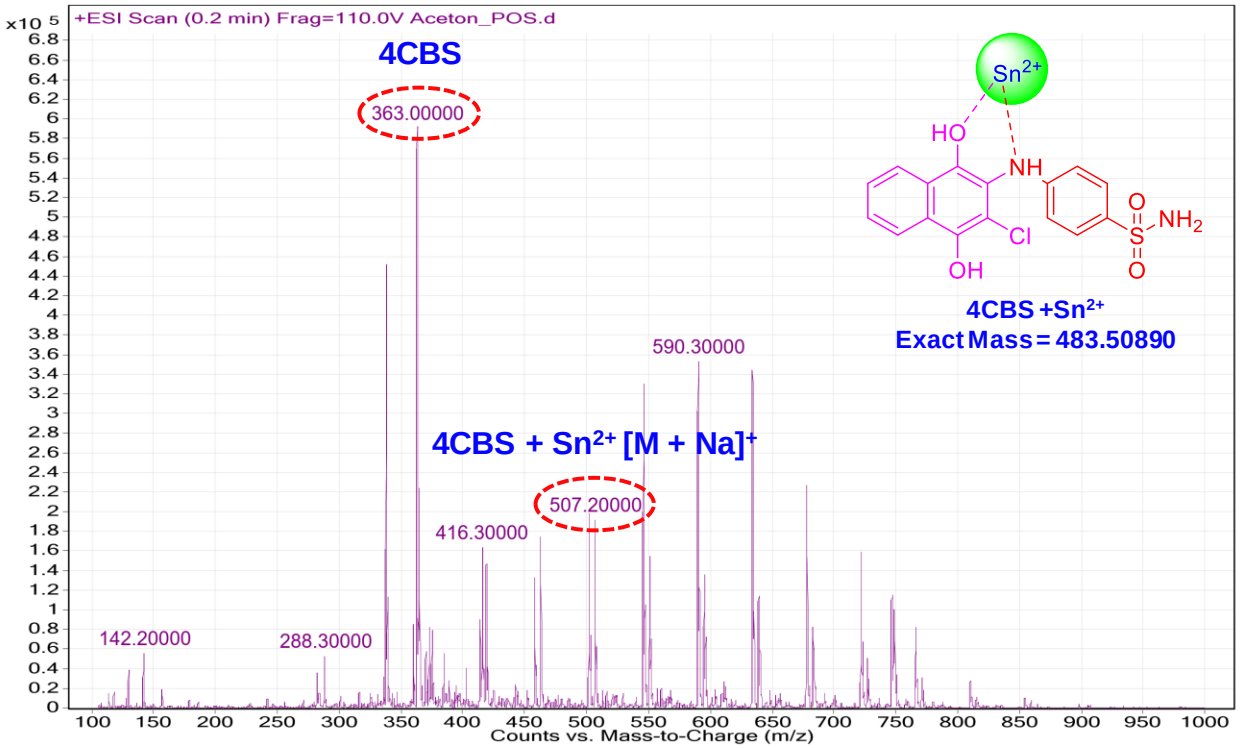

Figure S17. ESI–MS spectrum of **4CBS**–Sn^{2+} complex (1:1) in acetone. ESI-MS m/z calculated for **4CBS**–Sn^{2+}: 483.50890, found: 484.21024 $[M + Na]^+$.

Benesi-Hildebrand Plot of 4CBS–Sn^{2+} Complex

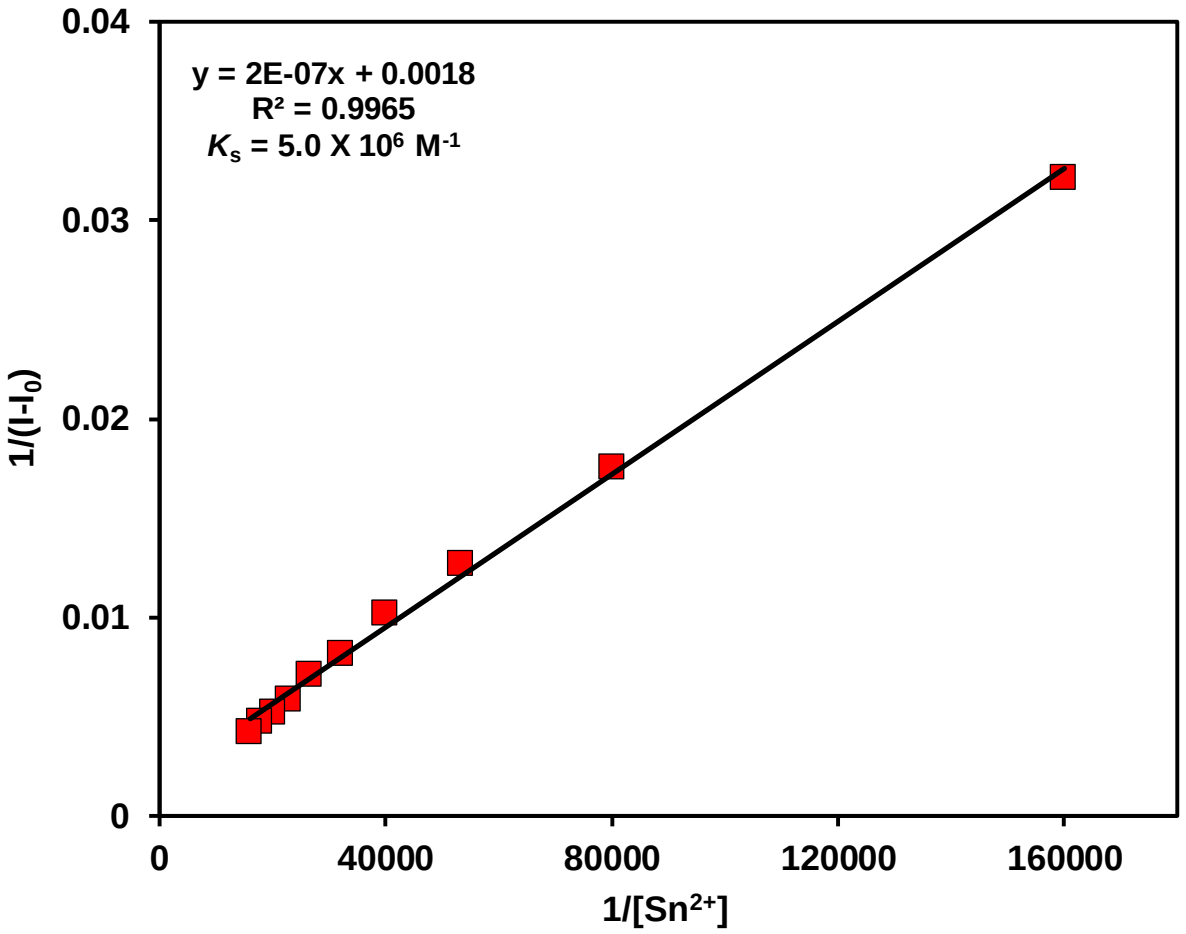

Figure S18. Benesi-Hildebrand plot for the determination of 1:1 binding stoichiometry of **4CBS**–Sn^{2+} complex.

Reversible Cycle Analysis of Chemosensing Probe 4CBS

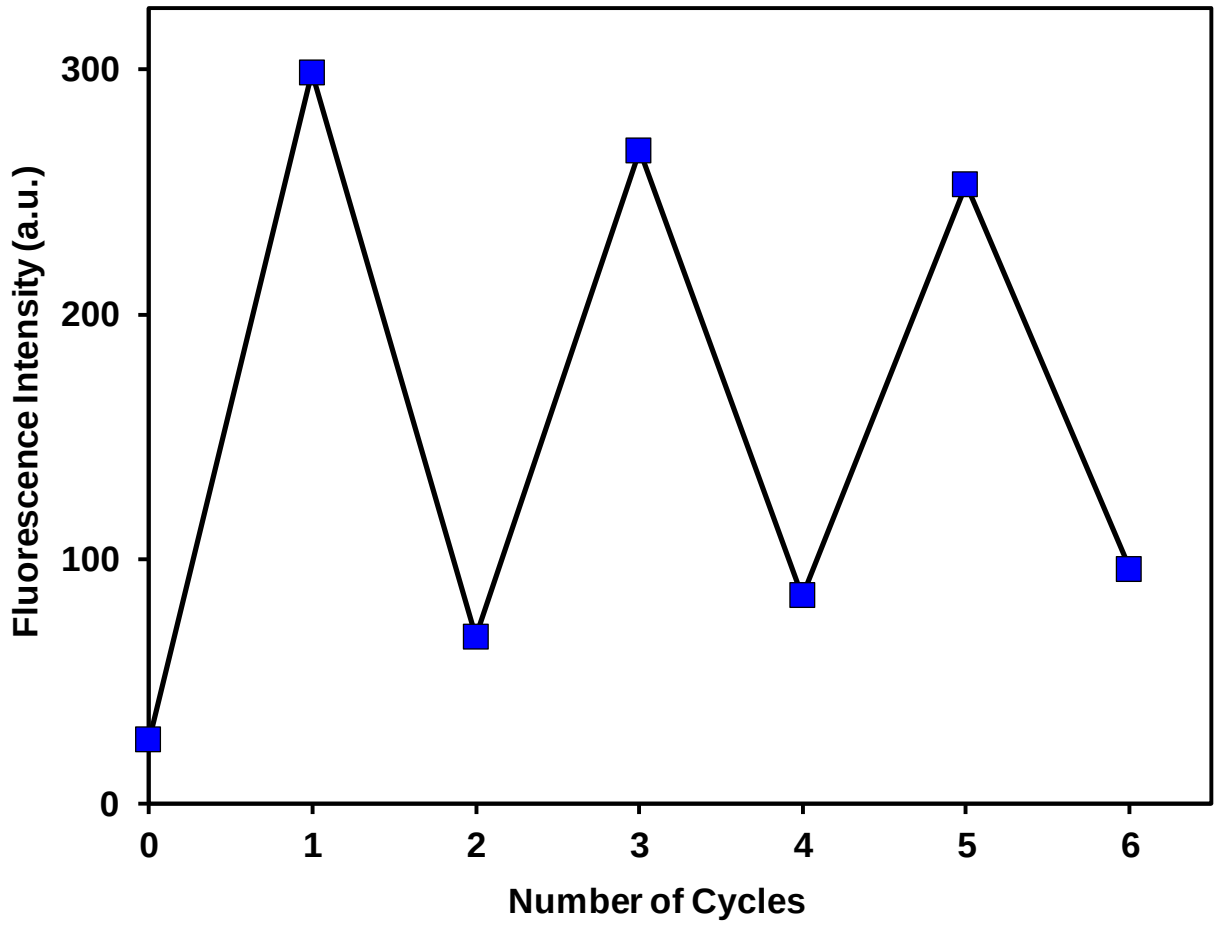

Figure S19. Reversibility cycle analysis of **4CBS** (1.25×10^{-5} M) with Sn^{2+} (6.25×10^{-5} M) in the presence of EDTA (1.75×10^{-3} M) in the aqueous solution (20 mM HEPES, pH = 7.5); λ_{ex} = 280 nm; λ_{em} = 397 nm.

Electrochemical Investigation of 4CBS–Sn^{2+} Complex

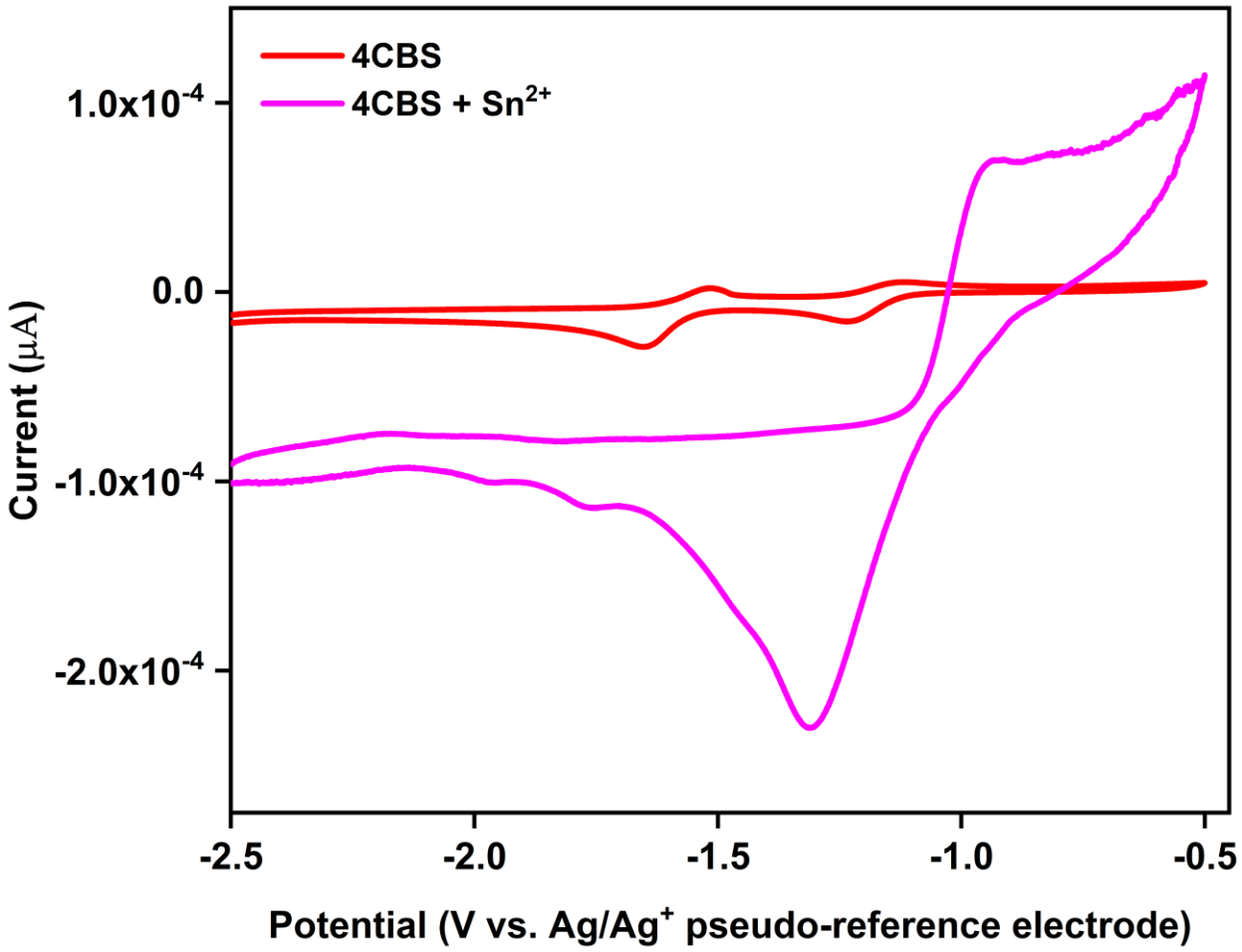

Figure S20. Cyclic voltammetry of 0.01 M **4CBS** and 0.01 M **4CBS** + Sn^{2+} in CH_3CN. 0.1 M TBATFB used as a supporting electrolyte. Ag/AgCl pseudo-reference electrode (non-aqueous), platinum wire (counter), and glassy carbon (working) electrodes were employed in this study. Potential range: -0.5 V up to -2.5 V at a scan rate of 0.1 V s^{-1}.

Optimized Structures of 4CBS and 4CBS–Sn^{2+} Complex

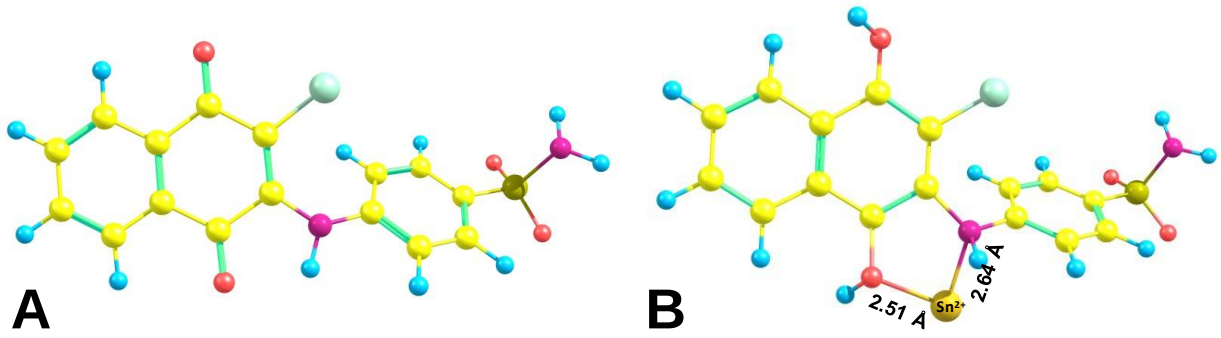

Figure S21. Optimized geometries of **4CBS** (A) and **4CBS**–Sn^{2+} complex (B).

Cytotoxicity Assay of 4CBS

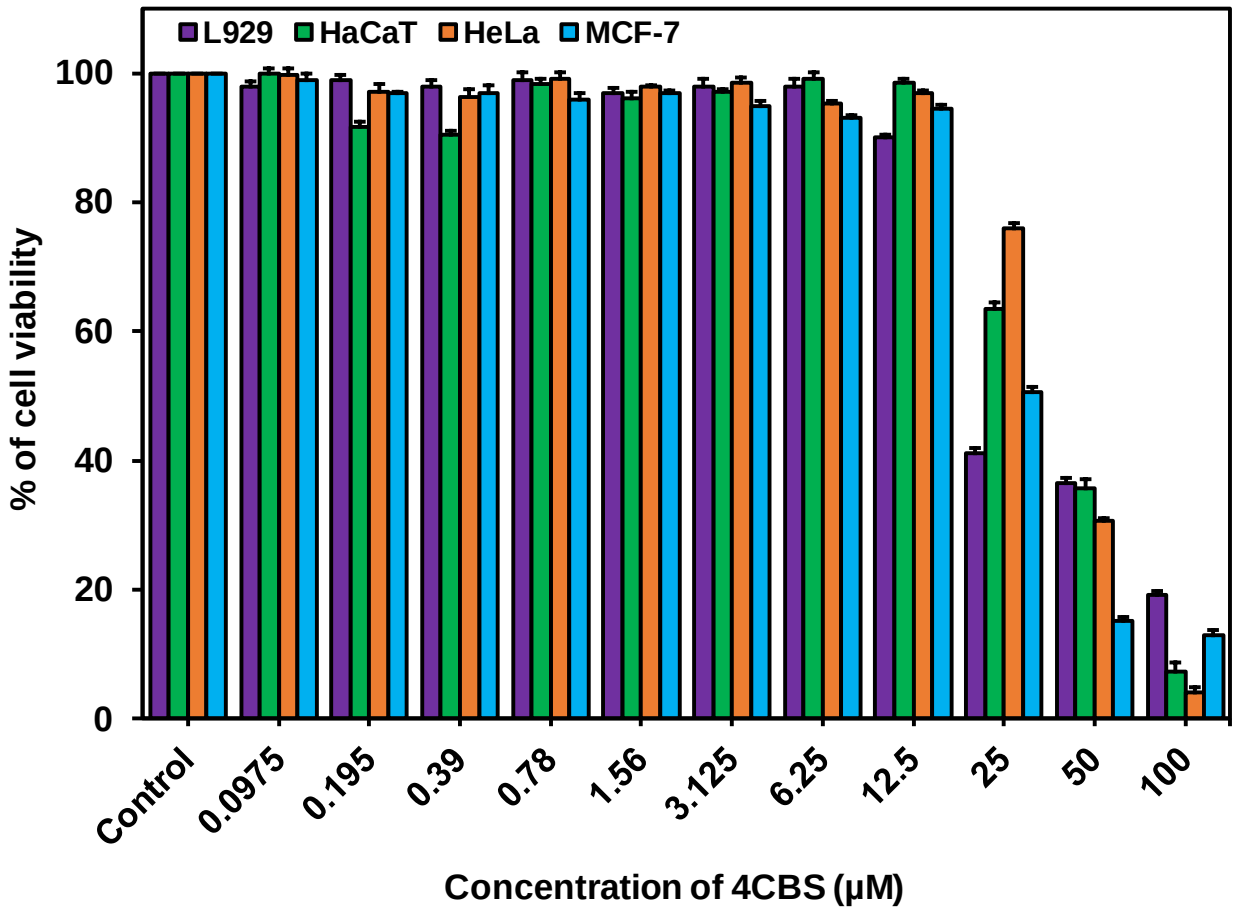

Figure S22. Cytotoxicity study of ligand **4CBS** against mouse fibroblast cells (L929), human keratinocyte cells (HaCaT), human cervical cancer cells (HeLa) and human breast cancer cells (MCF-7).

Discriminative Detection of Sn^{2+} in Live Cells

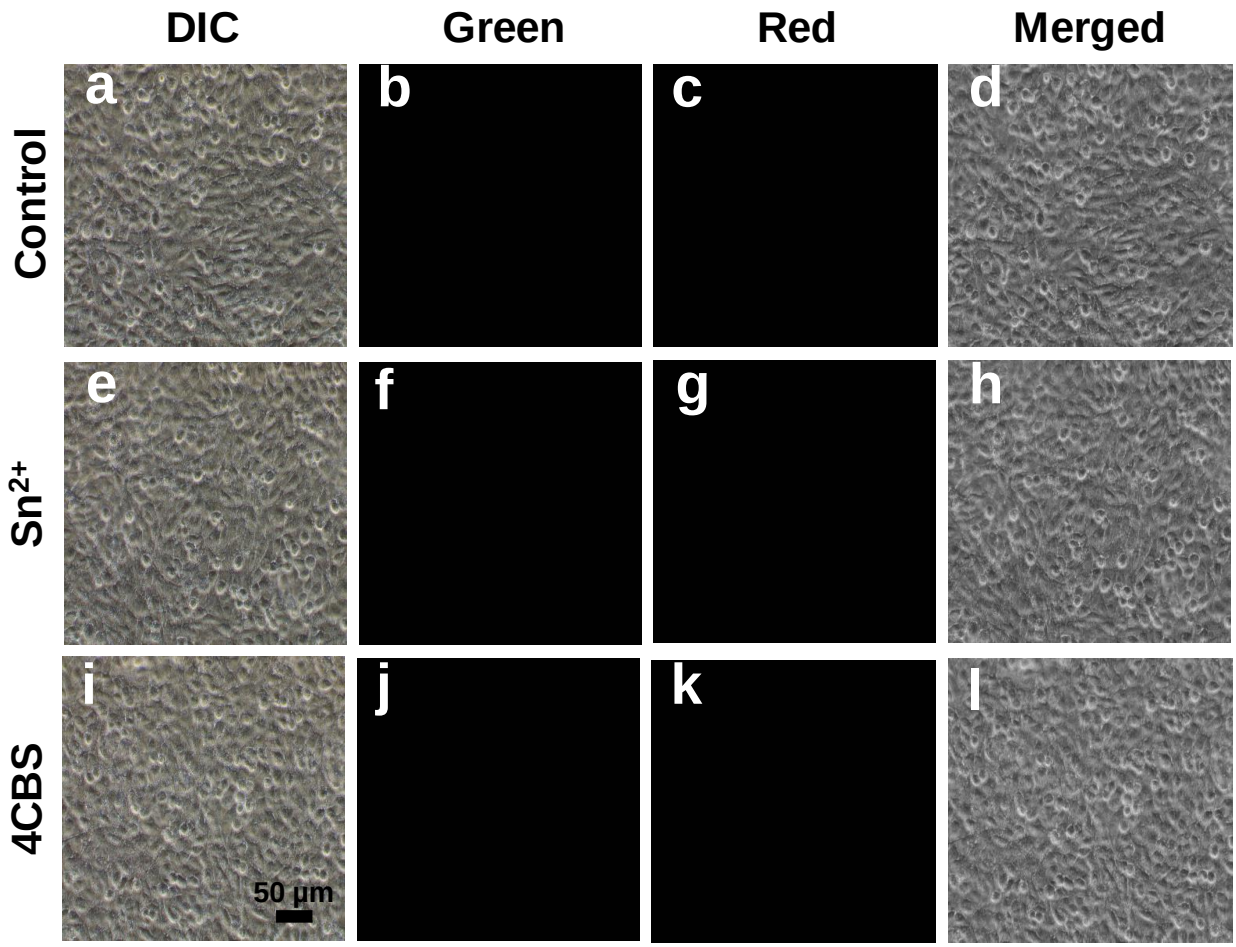

Figure S23. Fluorescence bioimaging of Sn^{2+} in L929 cells; where, images a–d = control cells; images e–h = cells treated with 6.25 µM Sn^{2+}; images i–l = cells treated with 6.25 µM **4CBS**.

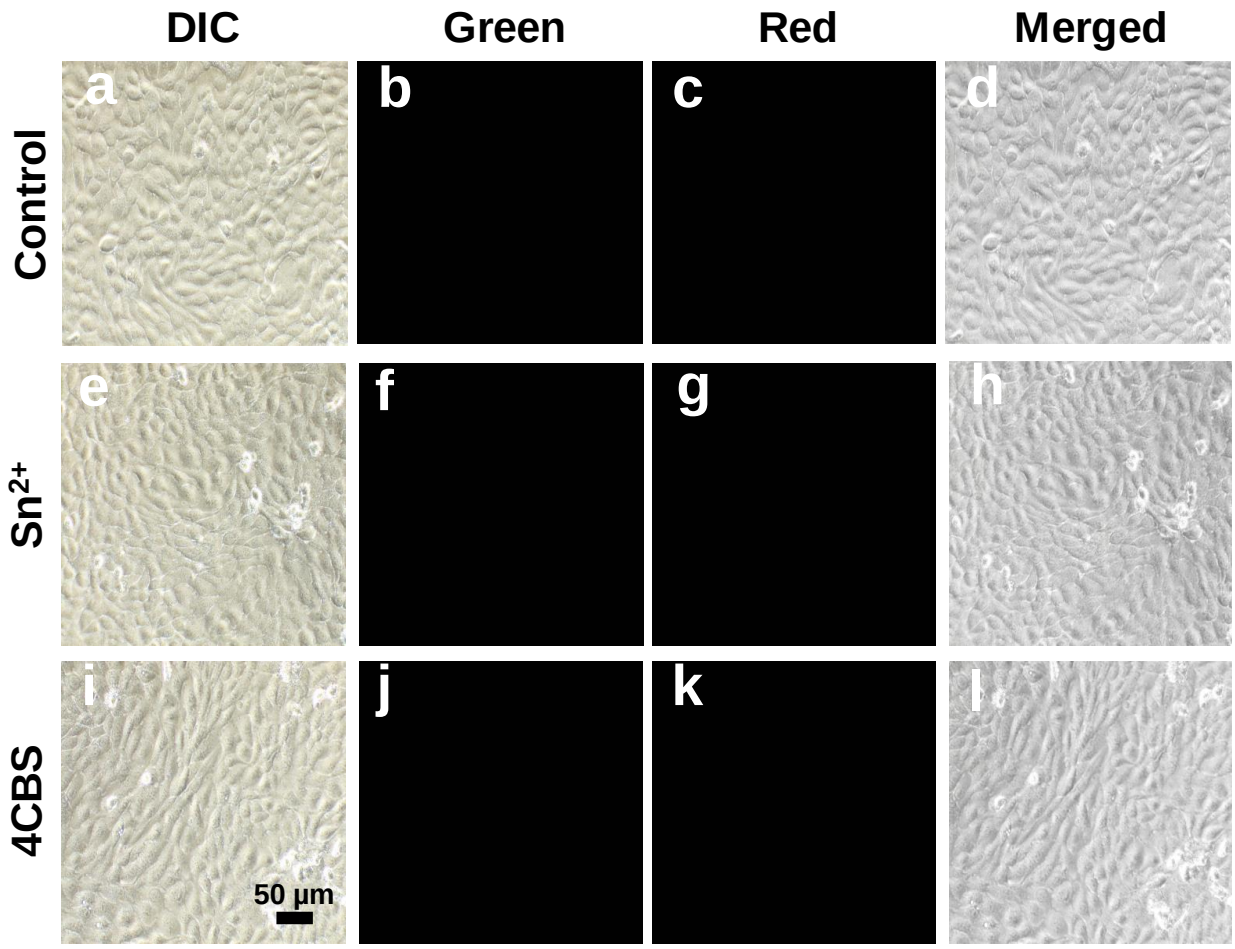

Figure S24. Fluorescence bioimaging of Sn^{2+} in HaCaT cells; where, images a–d = control cells; images e–h = cells treated with 6.25 µM Sn^{2+}; images i–l = cells treated with 6.25 µM **4CBS**.

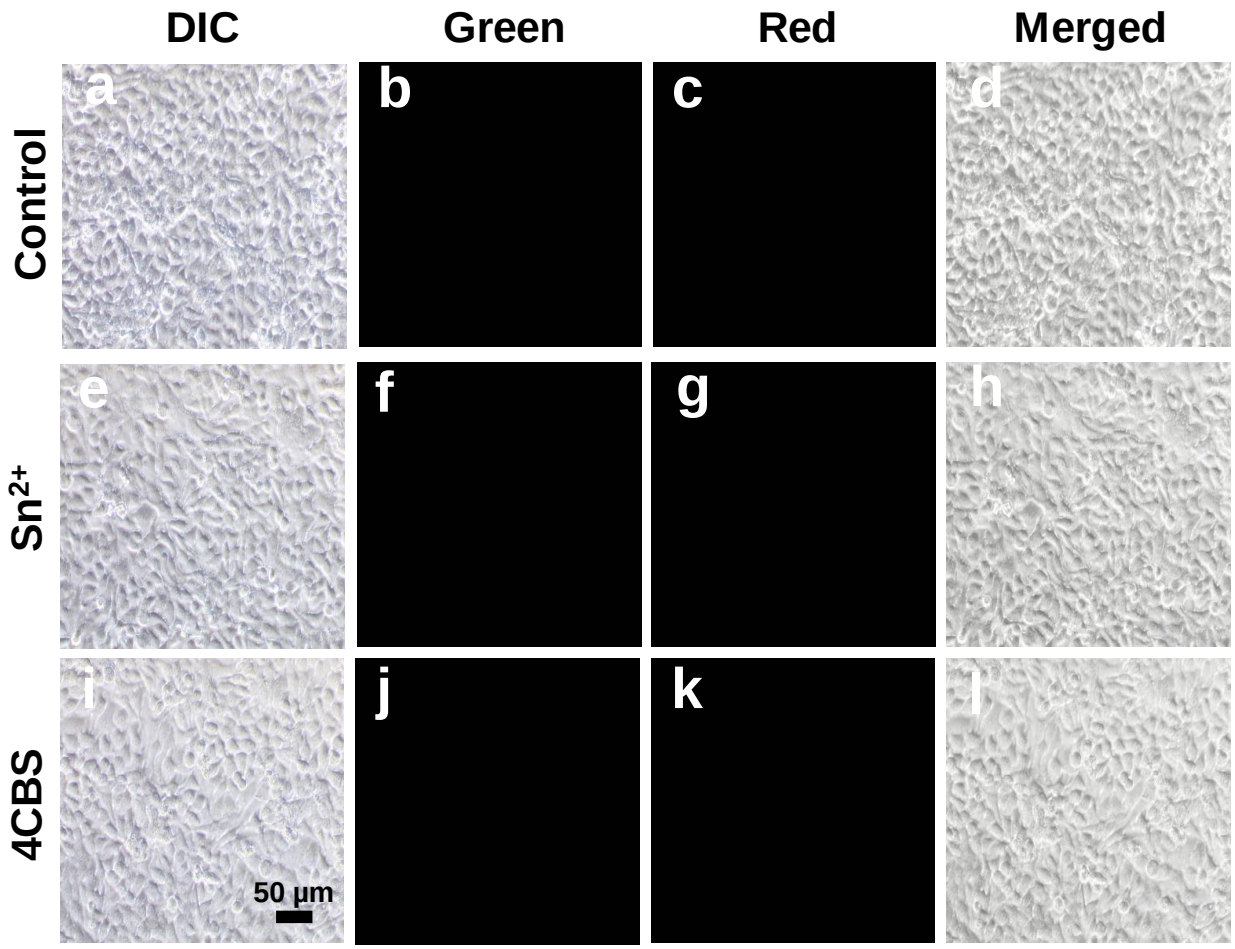

Figure S25. Fluorescence bioimaging of Sn^{2+} in HeLa cells; where, images a–d = control cells; images e–h = cells treated with 6.25 µM Sn^{2+}; images i–l = cells treated with 6.25 µM **4CBS**.

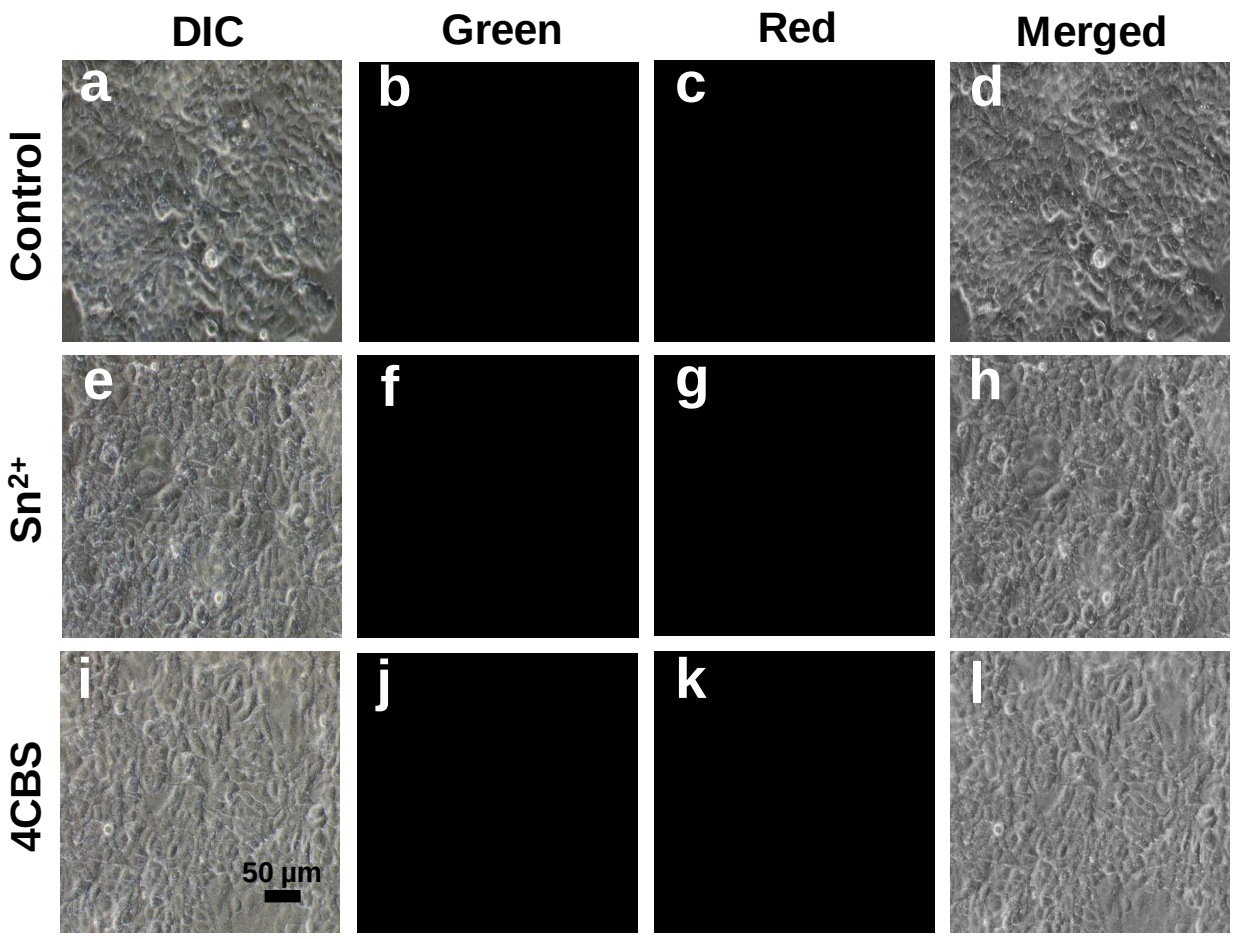

Figure S26. Fluorescence bioimaging of Sn^{2+} in MCF-7 cells; where, images a–d = control cells; images e–h = cells treated with 6.25 µM Sn^{2+}; images i–l = cells treated with 6.25 µM **4CBS**.

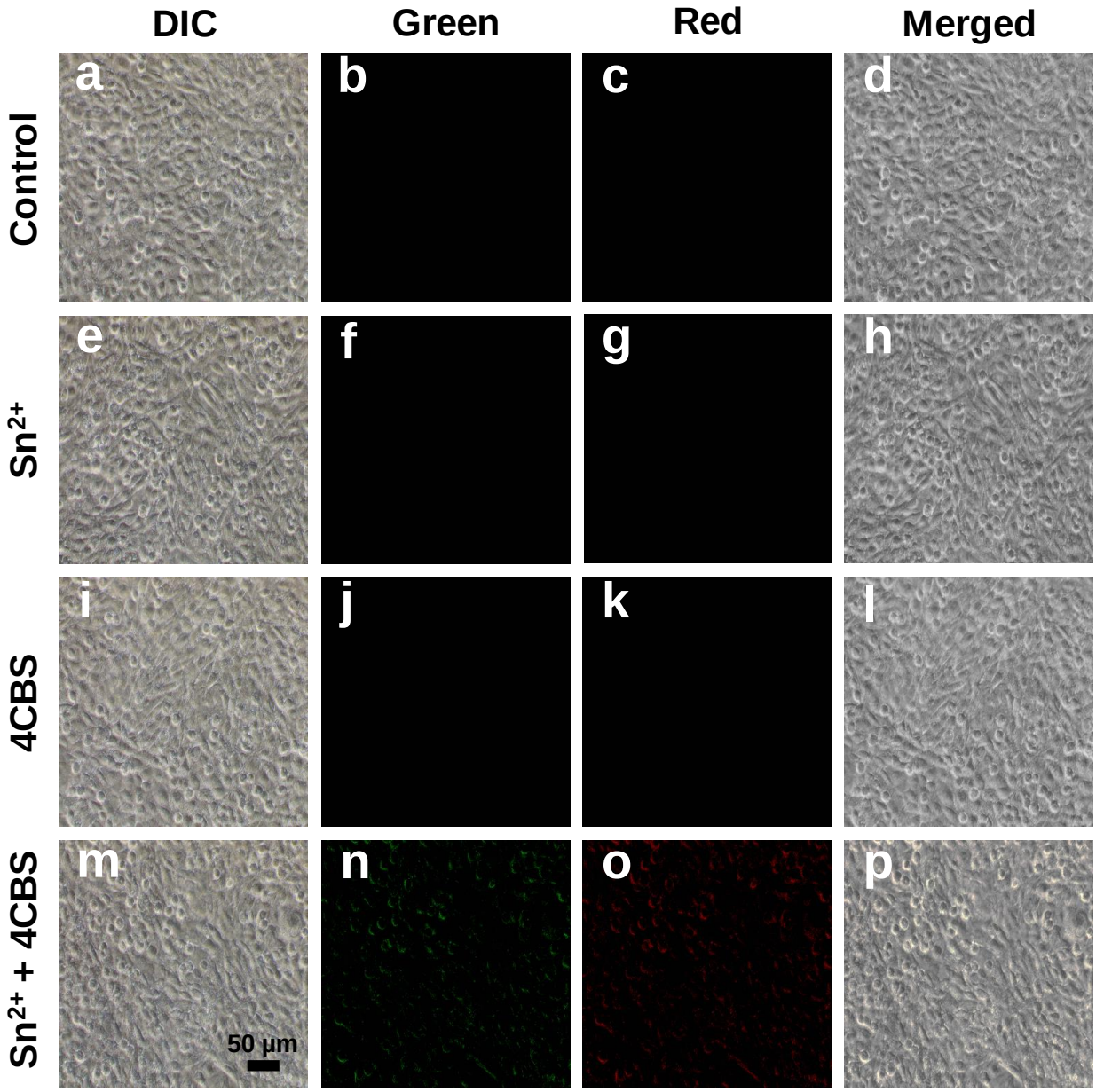

Figure S27. Fluorescence bioimaging of Sn^{2+} in L929 cells; where, images a–d = control cells; images e–h = cells treated with 12.50 µM Sn^{2+}; images i–l = cells treated with 12.50 µM **4CBS**; images m–p = cells treated with 12.50 µM Sn^{2+} and **4CBS**, respectively.

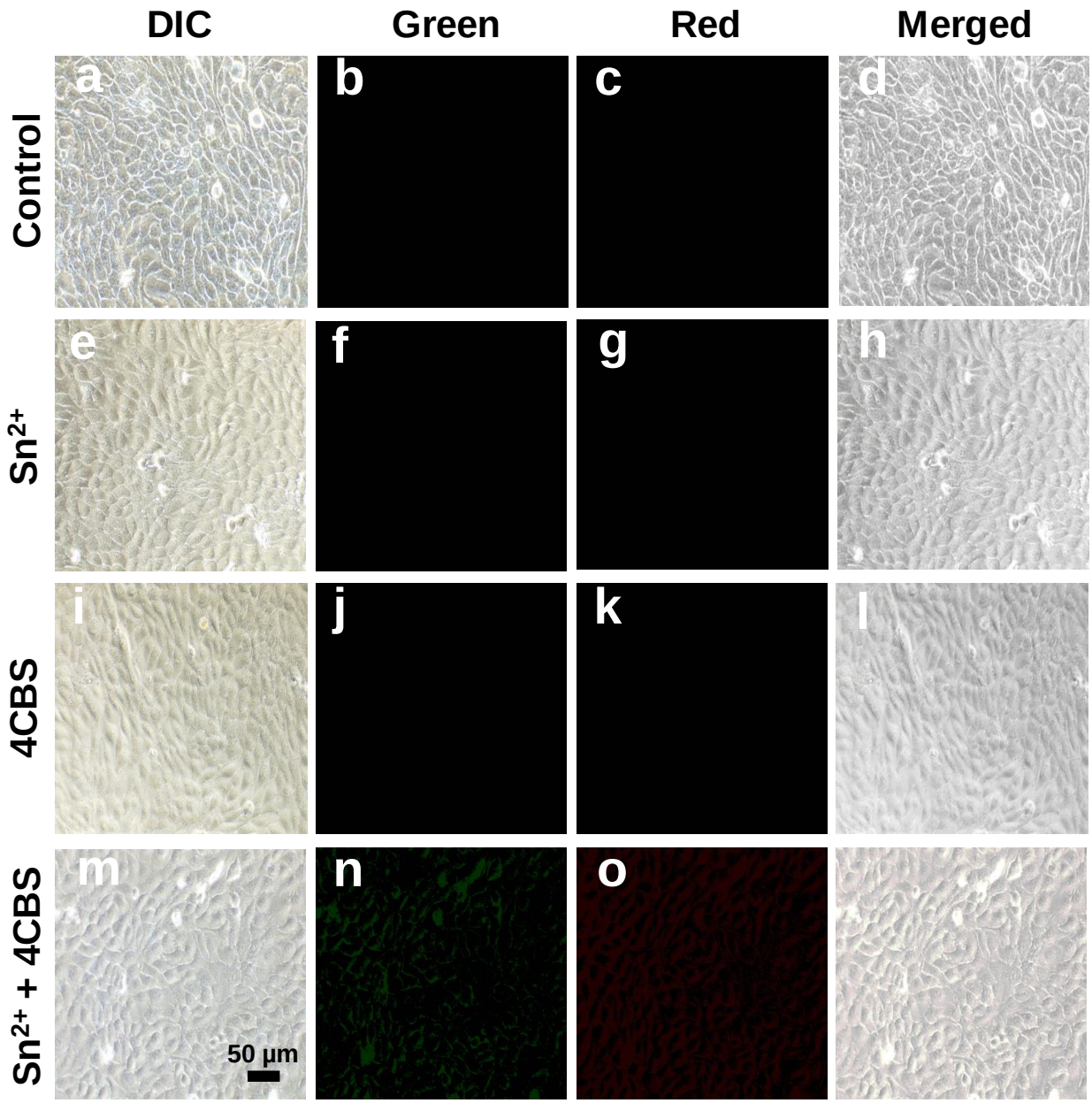

Figure S28. Fluorescence bioimaging of Sn^{2+} in HaCaT cells; where, images a–d = control cells; images e–h = cells treated with 12.50 µM Sn^{2+}; images i–l = cells treated with 12.50 µM **4CBS**; images m–p = cells treated with 12.50 µM Sn^{2+} and **4CBS**, respectively.

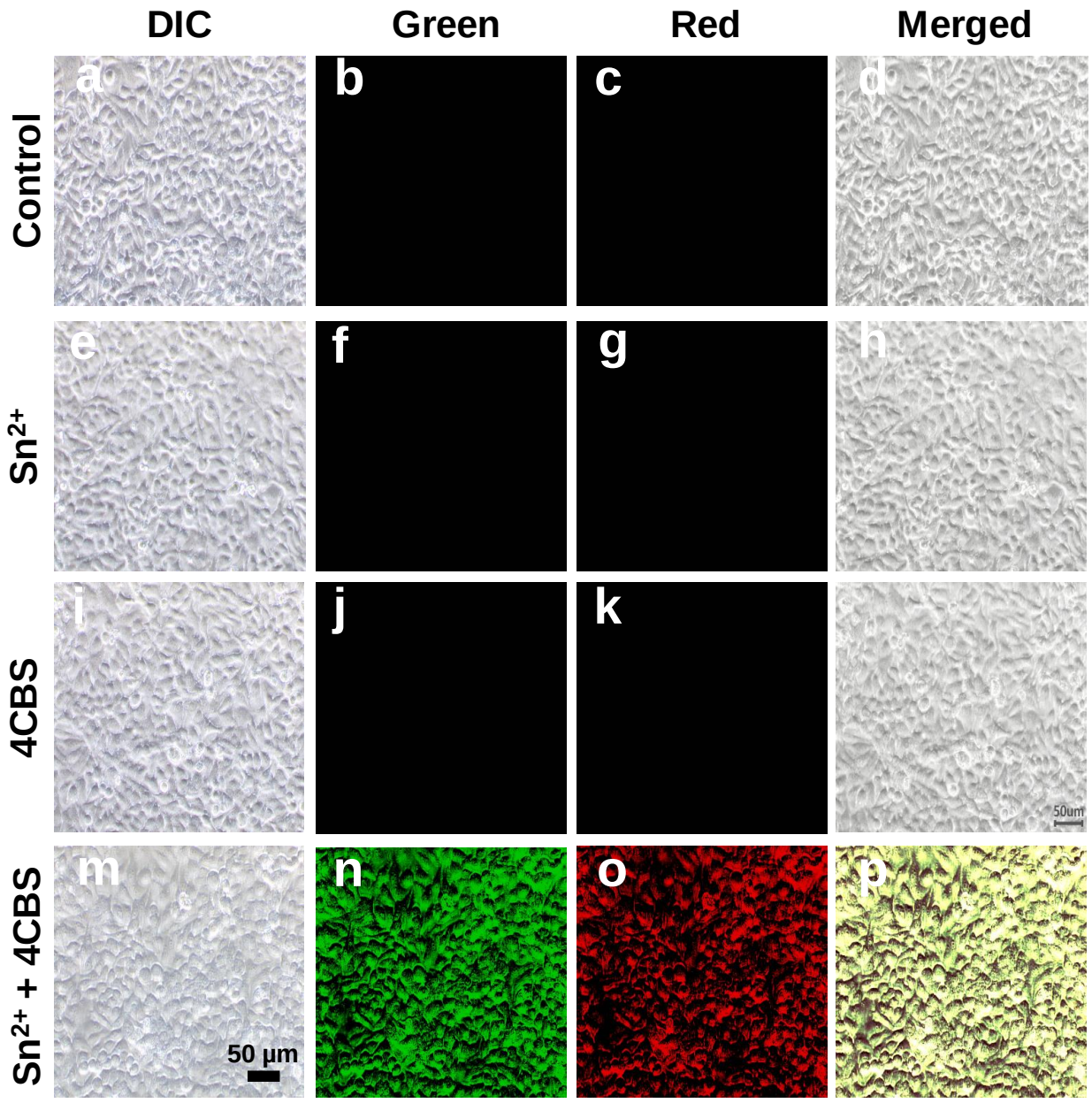

Figure S29. Fluorescence bioimaging of Sn^{2+} in HeLa cells; where, images a–d = control cells; images e–h = cells treated with 12.50 µM Sn^{2+}; images i–l = cells treated with 12.50 µM **4CBS**; images m–p = cells treated with 12.50 µM Sn^{2+} and **4CBS**, respectively.

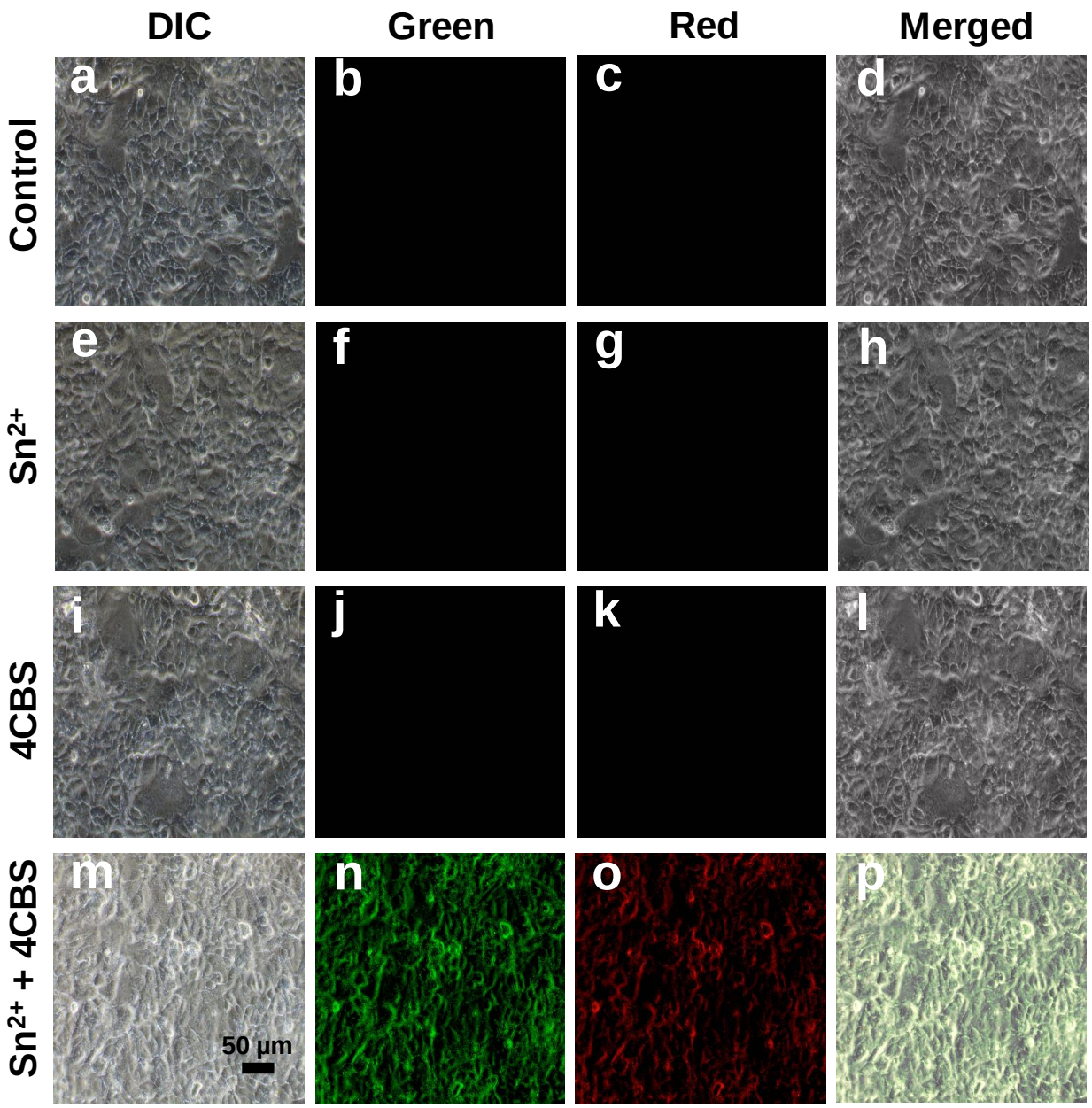

Figure S30. Fluorescence bioimaging of Sn^{2+} in MCF-7 cells; where, images a–d = control cells; images e–h = cells treated with 12.50 µM Sn^{2+}; images i–l = cells treated with 12.50 µM **4CBS**; images m–p = cells treated with 12.50 µM Sn^{2+} and **4CBS**, respectively.

Quantified Fluorescence Intensity in Live Cells

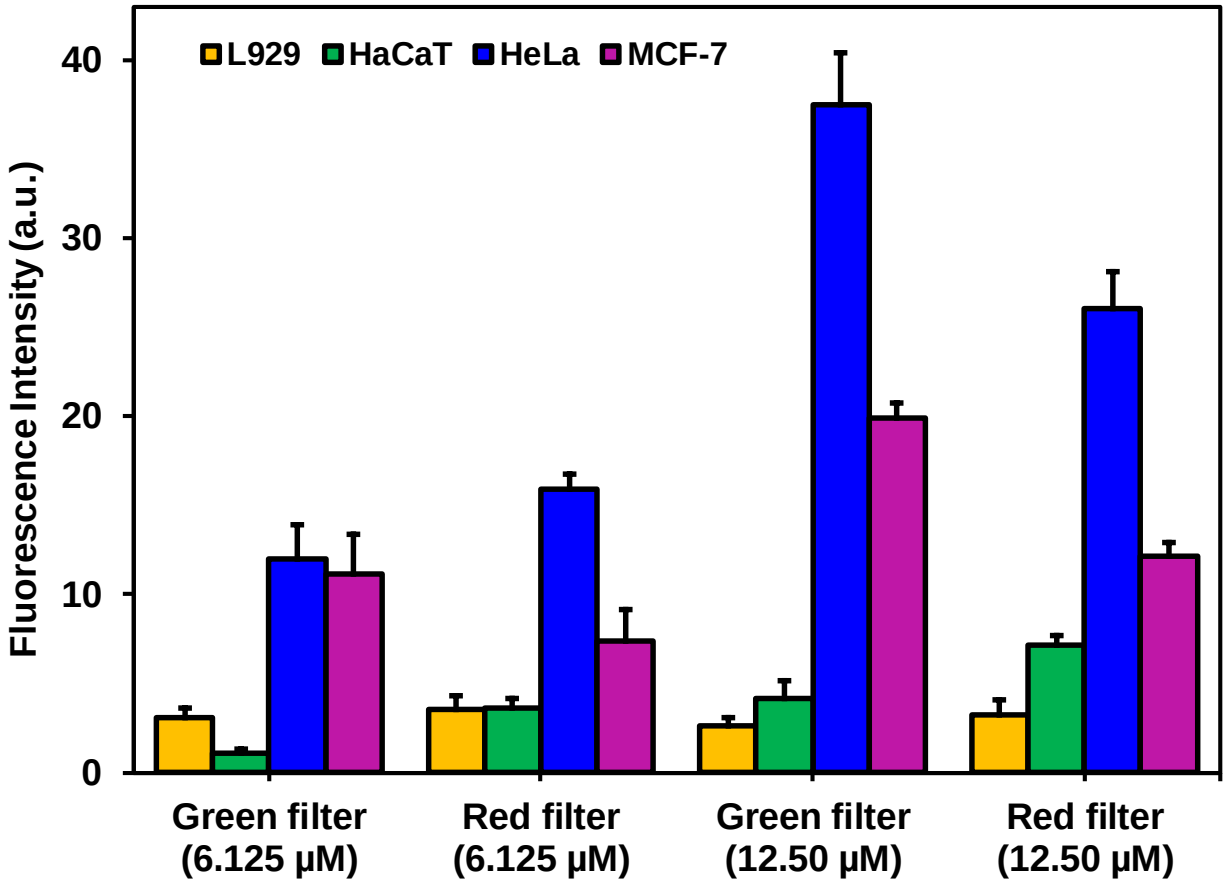

Figure S31. Quantified fluorescence intensity of live cells treated by Sn^{2+} and **4CBS**. The data represented as mean ± SD (n = 6); where n = quantification of the fluorescence signal from a number of fields of view.

Table S1. Comparative Analysis of Different Available Colorimetric/Fluorescence Chemosensing Probes for the Sensing of Sn^{2+}

S. No.	Ligand	Metal	Solvent	LOD & Complex stability constant (K_s)	Detection method	Color change	Application & probe concentration	Probe & metal incubation time	Ref.
1	Phenolphthalein-BODIPY derivative	Sn^{2+} & Al^{3+}	Acetone-H_2O (1:1)	6.31×10^{-8} M, 6.48×10^{-8} M & K_s not reported	Fluorescence spectroscopy	Maroon-yellow	Bioimaging in live cells, 5.0×10^{-5} M	1 h	[3]
2	Quinoline-substituted naphthothiazole	Sn^{2+} & Zn^{2+}	CH_3CN-H_2O (80/20, v/v)	8.21×10^{-8} M, 2.60×10^{-8} M & 7.5×10^{5} M^{-1} 15×10^{5} M^{-1}	Fluorescence spectroscopy	Colorless-yellow (Sn^{2+})	Bioimaging in live cells, 5.0×10^{-6} M	5 min & 1 h	[4]
3	Diarylethene with a carbazole unit	Sn^{2+} & Cu^{2+}	Methanol	1.9×10^{-6} M, 1.2×10^{-6} M & 4.04×10^{3} M^{-1} 3.40×10^{4} M^{-1}	Fluorescence spectroscopy	-	Real water sample analysis	-	[5]
4	N-Heterocyclic organosilatranes and their magnetic nanocomposites	Sn^{2+}	Methanol	4.8×10^{-6} M, 11.30×10^{4} M^{-1}	UV/vis & fluorescence spectroscopy	-	-	-	[6]
5	Chiral carbon dots-based nanosensors	Sn^{2+} & Lysine	DHP-CA buffer solution (pH = 7.4, 2.0 mL)	5.7×10^{-8} M, K_s not reported	Fluorescence spectroscopy	-	Bioimaging in live cells, 0.1 mg/mL	1 h	[7]
6	2-hydroxy-3-methoxy-5-[(*E*)-(4-nitrophenyl) diazenyl]benzaldehyde	Sn^{2+} & CN^{-}	CH_3CN-bis-tris buffer (9:1, v/v)	7.54×10^{-7} M, 6.49×10^{-7} M & 1.7×10^{3} M^{-1}	UV/vis spectroscopy	Yellow-colorless (Sn^{2+})	Real water sample analysis	-	[8]
7	Citrate stabilized silver nanoparticles	Sn^{2+}	Aqueous solution	4.0×10^{-8} M, K_s not reported	UV/vis spectroscopy	-	Real water sample analysis	-	[9]

8	Rhodamine-triazole-pyridine ternary conjugate	Sn^{2+}	CH_3CN-H_2O (99:1, v/v)	2.6×10^{-8} M & 1.2×10^{6} M^{-1}	Fluorescence spectroscopy	Colorless-pink	Real water sample analysis		[10]
9	(2-(2-hydroxyphenyl)-1*H*–benzo[*d*]imidazol-5-yl)(phenyl)methanone	Sn^{2+}	THF-HEPES buffer (90:10, v/v)	3.28×10^{-12} M & 1.50×10^{4} M^{-1}	Fluorescence spectroscopy	-	-		[11]
10	4-(Naphthalen-1-ylethynyl) aniline appended rhodamine	Sn^{2+}	CH_3CN-HEPES (1.0×10^{-5} M, 1:4, v/v)	5.0×10^{-9} M & 3.1×10^{5} M^{-1}	Fluorescence spectroscopy	-	Bioimaging in live cells, 1.0×10^{-5} M	2 h & 1 h	[12]
11	**4CBS**	**Sn^{2+}**	**H_2O (20 mM HEPES, pH = 7.5)**	**1.15×10^{-7} M & 5.0×10^{6} M^{-1}**	**Colorimetric & Fluorescence spectroscopy**	**Light maroon-milky white**	**Discriminative bioimaging in live cells and bioimaging in zebrafish, 6.25×10^{-6} M**	**10 min**	**This work**

References

(1) Frisch, M. J.; Trucks, G. W.; Schlegel, H. B.; Scuseria, G. E.; Robb, M. A.; Cheeseman, J. R.; Scalmani, G.; Barone, V.; Petersson, G. A.; Nakatsuji, H.; Li, X.; Caricato, M.; Marenich, A. V.; Bloino, J.; Janesko, B. G.; Gomperts, R.; Mennucci, B.; Hratchian, H. P.; Ortiz, J. V.; Izmaylov, A. F.; Sonnenberg, J. L.; Williams; Ding, F.; Lipparini, F.; Egidi, F.; Goings, J.; Peng, B.; Petrone, A.; Henderson, T.; Ranasinghe, D.; Zakrzewski, V. G.; Gao, J.; Rega, N.; Zheng, G.; Liang, W.; Hada, M.; Ehara, M.; Toyota, K.; Fukuda, R.; Hasegawa, J.; Ishida, M.; Nakajima, T.; Honda, Y.; Kitao, O.; Nakai, H.; Vreven, T.; Throssell, K.; Montgomery Jr., J. A.; Peralta, J. E.; Ogliaro, F.; Bearpark, M. J.; Heyd, J. J.; Brothers, E. N.; Kudin, K. N.; Staroverov, V. N.; Keith, T. A.; Kobayashi, R.; Normand, J.; Raghavachari, K.; Rendell, A. P.; Burant, J. C.; Iyengar, S. S.; Tomasi, J.; Cossi, M.; Millam, J. M.; Klene, M.; Adamo, C.; Cammi, R.; Ochterski, J. W.; Martin, R. L.; Morokuma, K.; Farkas, O.; Foresman, J. B.; Fox, D. J. *Gaussian 16 Rev. C.01*, Wallingford, CT, 2016.

(2) Becker, H.; Berger, W.; Domschke, G.; Fanghänel, E.; Faust, J.; Fischer, M.; Gentz, F.; Gewald, K.; Gluch, R.; Mayer, R.; Müller, K.; Pavel, D.; Schmidt, H.; Schollberg, K.; Schwetlick, K.; Zeppenfeld, G. In *Organicum*, Becker, H.; Berger, W.; Domschke, G.; Fanghänel, E.; Faust, J.; Fischer, M.; Gentz, F.; Gewald, K.; Gluch, R.; Mayer, R.; Müller, K.; Pavel, D.; Schmidt, H.; Schollberg, K.; Schwetlick, K.; Zeppenfeld, G., Eds.; Pergamon, 1973, pp 607-664.

(3) Gul, A.; Oguz, M.; Kursunlu, A. N.; Yilmaz, M. *Dyes Pigm.* **2020**, *176*, 108221.

(4) Jonaghani, M. Z.; Zali-Boeini, H.; Taheri, R.; Rudbari, H. A.; Askari, B. *RSC Adv.* **2016**, *6*, 34940-34945.

(5) Qu, S.; Zheng, C.; Liao, G.; Fan, C.; Liu, G.; Pu, S. *RSC Adv.* **2017**, *7*, 9833-9839.

(6) Singh, G.; Diksha; Singh, A.; Sanchita; Sharma, G.; Shilpy; Pawan; Espinosa-Ruíz, C.; Esteban, M. A. *New J. Chem.* **2020**, *44*, 6238-6250.

(7) Gao, P.; Xie, Z.; Zheng, M. *Sens. Actuators, B* **2020**, *319*, 128265.

(8) Dongare, P. R.; Gore, A. H.; Ajalkar, B. D. *Inorg. Chim. Acta* **2020**, *502*, 119372.

(9) Salem, J. K.; El Nahhal, I. M.; H. Shurrab, M. *Int. J. Environ. Anal. Chem.* **2020**, 1-11.

(10) Yan, Z.; Wei, G.; Guang, S.; Xu, M.; Ren, X.; Wu, R.; Zhao, G.; Ke, F.; Xu, H. *Dyes Pigm.* **2018**, *159*, 542-550.

(11) Jadhav, A. G.; Shinde, S. S.; Lanke, S. K.; Sekar, N. *Spectrochim. Acta, Part A* **2017**, *174*, 291-296.

(12) Adhikari, S.; Ghosh, A.; Guria, S.; Sahana, A. *RSC Adv.* **2016**, *6*, 39657-39662.